Atmos. Chem. Phys., 26, 11153–11169, 2026
https://doi.org/10.5194/acp-26-11153-2026

Atmospheric Chemistry and Physics
Open Access
EGU

Exploring the hydrogen abstraction pathway in HOM formation from α-pinene photooxidation systems under varying NO conditions

Hui Wang[1,★], Hongru Shen[2,★], Defeng Zhao[3,4], Sungah Kang[1], Rongrong Wu[5], Yarê Baker[6], Quanfu He[7], Annika Zanders[1], Mathias Bachner[8], Douglas R. Worsnop[9,10], Thorsten Hohaus[1], Thomas F. Mentel[1,☆], and Sören R. Zorn[1]

[1]Institute of Climate and Energy Research, ICE-3: Troposphere, Forschungszentrum Jülich, 52425 Jülich, Germany
[2]School of Environmental Science and Engineering, Shanghai Jiao Tong University, Shanghai 200240, P. R. China
[3]Shanghai Frontiers Science Center of Atmosphere-Ocean Interaction, Department of Atmospheric and Oceanic Sciences & Institute of Atmospheric Sciences, Fudan University, Shanghai 200438, China
[4]Institute of Eco-Chongming (IEC), 20 Cuiniao Rd., Chongming, Shanghai, 202162, China
[5]Centre for Atmospheric Sciences, School of Earth, Atmospheric & Environmental Sciences, University of Manchester, M13 9PL Manchester, United Kingdom
[6]Leibniz Institute for Tropospheric Research (TROPOS), 04318 Leipzig, Germany
[7]Earth, Ocean and Atmospheric Sciences (EOAS) Thrust, Function Hub, The Hong Kong University of Science and Technology (Guangzhou), 511458 Guangzhou, Guangdong, China
[8]Institute of Technology and Engineering, Forschungszentrum Jülich, 52425 Jülich, Germany
[9]Institute for Atmospheric and Earth System Research/Physics, Faculty of Science, University of Helsinki, 00560 Helsinki, Finland
[10]Aerodyne Research, Inc., Billerica, 01821 Massachusetts, United States
☆retired
★These authors contributed equally to this work.

Correspondence: Defeng Zhao (dfzhao@fudan.edu.cn) and Sören R. Zorn (s.zorn@fz-juelich.de)

Received: 26 February 2026 – Discussion started: 1 April 2026
Revised: 30 June 2026 – Accepted: 20 July 2026 – Published: 10 August 2026

Abstract. Highly oxygenated organic molecules (HOM) are formed via autoxidation during •OH-initiated oxidation of α-pinene. We investigated the relative contributions of OH-addition and hydrogen (H)-abstraction to HOM formation from α-pinene photooxidation under varying nitrogen oxide (NO) conditions. HOM molecules were detected by a nitrate chemical ionization mass spectrometer (CIMS). In the absence of NO, $C_{10}H_{17}O_x$• peroxy radicals and related termination products (e.g. $C_{10}H_{18}O_x$) dominated the HOM spectrum, accounting for $>70\,\%$ of total HOM. The presence of NO substantially altered HOM products, particularly by rapid formation of $C_{10}H_{15}O_x$•-related HOM, like $C_{10}H_{15}NO_8$. The ratio of $C_{10}H_{15}NO_x$ to $C_{10}H_{17}NO_x$ increased from 0.34 to 0.84 as the RO_2• loss rate via reaction with NO increased from 0.18 to $1.06\,s^{-1}$. Under high-NO conditions, $C_{10}H_{15}O_x$•-related HOM contributed up to 34 % to total HOM from α-pinene oxidation systems. The H-abstraction channel proved to be the source of $C_{10}H_{15}O_x$•-related HOM. Fuzzy *c*-means clustering indicated that $C_{10}H_{15}O_x$•-related HOM exhibited the fastest formation rate among the identified HOM groups, consistent with first-generation products. Comparison with pinonaldehyde oxidation, obtained by normalizing HOM yields to pinonaldehyde turnover, suggests that pinonaldehyde contributed $\sim 5\,\%$ of HOM in α-pinene systems,

excluding secondary oxidation as the dominant source. Detection of $C_{10}H_{15}NO_4$ under high-NO conditions by propylamine-CIMS indicates the formation of $C_{10}H_{15}O_3\bullet$ peroxy radicals, formed by alkoxy radical decomposition and six-membered ring opening in the H-abstraction channel. This study highlights the role of the H-abstraction pathway in •OH-initiated α-pinene oxidation under NO-influenced conditions and provides new constraints on detailed HOM formation mechanisms.

1 Introduction

Secondary organic aerosols (SOA) in the atmosphere contribute significantly to particulate matter in the PM_1 size range and can affect regional air quality, human health and global radiative forcing (Jimenez et al., 2009; Peng et al., 2016). The oxidation of biogenic volatile compounds (BVOC) contributes significantly to the total formed SOA. Highly oxygenated organic compounds (HOM) are produced via autoxidation of peroxy radicals ($RO_2\bullet$). They typically contain at least six oxygen atoms and consequently show a low to extremely low volatility. This enables them to nucleate or to condense onto existing particles and thus to significantly contribute to SOA formation (Bianchi et al., 2019; Mentel et al., 2015; Ehn et al., 2014).

α-pinene is globally the most abundant monoterpene and has been shown to form significant amounts of HOM when it is oxidized by O_3 or by hydroxyl radicals (•OH) (Ehn et al., 2014; Berndt et al., 2016). •OH initiated oxidation of α-pinene occurs via the OH-addition pathway ($\sim 90\,\%$) and the hydrogen (H)-abstraction pathway ($\sim 10\,\%$), leading to the formation of peroxy radicals ($RO_2\bullet$) with the formulas $C_{10}H_{17}O_3\bullet$ and $C_{10}H_{15}O_2\bullet$, respectively (Vereecken et al., 2007).

The OH-addition pathway is known to effectively form HOM with fast rates when the four-membered ring is broken (Berndt, 2021; Xu et al., 2019). However, the potential role of the H-abstraction pathway for HOM formation has received far less attention and was thought to be negligible until Shen and coworkers suggested its significant contribution to HOM (Shen et al., 2022). In addition, Luo et al. (2023) also highlighted the significance of H-abstraction to HOM formation from limonene photooxidation in the presence of NO. Therefore, the H-abstraction pathway can be a potential explanation for the observations in Hyytiälä where $C_{10}H_{15}O_x\bullet$-related HOM species (e.g. $C_{10}H_{15}NO_8$) are dominant and have been identified as fingerprints of daytime oxidation (Yan et al., 2016). However, confirmation and clarification of the contribution of the H-abstraction pathway to HOM formation are still required. In the study by Shen et al. (2022) the potential role of the conversion of pinonaldehyde to $C_{10}H_{15}O_x\bullet$ species was only estimated and not directly measured. The extent to which pinonaldehyde oxidation contributes to $C_{10}H_{15}O_x\bullet$-related HOM in α-pinene systems remains uncertain.

The detection of $C_{10}H_{15}O_x\bullet$ related products with fewer than five oxygen atoms suggests contributions from H-abstraction pathways. However, Shen et al. (2022) reported only HOM with oxygen numbers greater than six, and NO was present in all experiments performed (Shen et al., 2022). The presence or absence of NO can have a significant impact, as it strongly influences the rearrangement of alkoxy radicals, which is crucial to facilitate HOM formation via the H-abstraction pathway (Shen et al., 2022). Therefore, systematic experiments under varying NO conditions, especially including NO-free conditions, are essential for confirming the occurrence of the H-abstraction pathway, to elucidate its product distribution, and to clarify its role in HOM and subsequent SOA formation in α-pinene photooxidation systems.

Competition between termination pathways of $C_{10}H_{17}O_x\bullet$ and $C_{10}H_{15}O_x\bullet$ peroxy radicals determines the product distributions (Mentel et al., 2015). All products are separated into various families based on the numbers of carbon atoms, hydrogen atoms and oxygen atoms. The $C_{10}H_{18}O_x$ family, which includes compounds containing ten carbon atoms, eighteen hydrogen atoms, and a varying number of oxygen atoms with hydroperoxide or alcohol functions, can only be attributed to $C_{10}H_{17}O_x\bullet$ via termination either by $HO_2\bullet$ radicals (Reaction R1) or by other peroxy radicals ($R'O_2\bullet$) via Reaction (R3) (Baker et al., 2024). Similarly, the organic nitrate $C_{10}H_{17}NO_x$ family is formed via the reaction of $C_{10}H_{17}O_x\bullet$ with NO (Reaction R6) (Berndt, 2021). The $C_{10}H_{14}O_x$ family, comprising carbonyl containing compounds, is generated either via reactions of $C_{10}H_{15}O_x\bullet$ with $R'O_2\bullet$ or via self-termination (Reaction R8) (Rissanen et al., 2014). In the atmosphere, alkoxy radicals with the formula $C_{10}H_{15}O_{x-1}\bullet$ are mainly products of the reaction between $C_{10}H_{15}O_x\bullet$ and NO (Reaction R2) (Berndt, 2021). The $C_{10}H_{15}NO_x$ family is uniquely attributed to the reaction of $C_{10}H_{15}O_x\bullet$ peroxy radicals with NO (Reaction R6). Thus, the appearance of HOM with formulas $C_{10}H_{18}O_x$ and $C_{10}H_{17}NO_x$ can clearly be traced to $C_{10}H_{17}O_x\bullet$, while $C_{10}H_{14}O_x$ and $C_{10}H_{15}NO_x$ are clearly related to $C_{10}H_{15}O_x\bullet$. The formation of the $C_{10}H_{16}O_x$ family can occur via multiple pathways including termination reactions of $C_{10}H_{15}O_x\bullet$ with $HO_2\bullet$ or $R'O_2\bullet$, termination of $C_{10}H_{17}O_x\bullet$ with $R'O_2\bullet$, or self-termination of $C_{10}H_{17}O_x\bullet$. The important initiation of reactions is shown in Fig. S1 in the Supplement, and termination pathways of $RO_2\bullet$ and corresponding products are

shown below in Fig. 1.

$$RO_2\bullet + HO_2\bullet \rightarrow ROOH + O_2 \quad (R1)$$
$$RO_2\bullet + HO_2\bullet \rightarrow RO\bullet + \bullet OH + O_2 \quad (R2)$$
$$RO_2\bullet + R'O_2\bullet \rightarrow R{=}O + R'OH + O_2 \quad (R3)$$
$$RO_2\bullet + R'O_2\bullet \rightarrow RO\bullet + R'O\bullet + O_2 \quad (R4)$$
$$RO_2\bullet + R'O_2\bullet \rightarrow ROOR' + O_2 \quad (R5)$$
$$RO_2\bullet + NO \rightarrow RONO_2 \quad (R6)$$
$$RO_2\bullet + NO \rightarrow RO\bullet + NO_2 \quad (R7)$$
$$RO_2\bullet \rightarrow R{=}O + \bullet OH \quad (R8)$$

In our study we conducted systematic experiments of α-pinene photooxidation under varying NO concentrations to investigate the role of the H-abstraction pathway in HOM formation. We focused on early reaction stages, which means the first minutes after •OH generation by photolysis of H_2O_2, to capture primary generation product distributions, during which only autoxidation and reaction with NO were the two dominant reaction pathways for $RO_2\bullet$. Fuzzy *c*-means clustering was applied to distinguish $C_{10}H_{15}O_x\bullet$-related HOM from other products based on their formation pathways. To elucidate the role of secondary oxidation, pinonaldehyde was investigated under identical conditions, and the results were compared with the α-pinene system. Both less oxygenated and highly oxygenated products were detected by employing propylamine and nitrate reagents in chemical ionization mass spectrometry (CIMS).

Combination of the results provides complementary and consistent insights into product distributions and formation pathways, highlighting the importance of the H-abstraction pathway to produce HOM and subsequently contribute to SOA formation. The results demonstrate that the H-abstraction pathway is an important process generating product distributions highlighting its potential contribution to HOM and SOA formation.

2 Experiments and Methods

2.1 Simulation experiments in SAPHIR STAR

The experiments were conducted in SAPHIR-STAR, a 2 m^3 continuously stirred tank reactor (SAPHIR: **S**imulation of **A**tmospheric **PH**otochemistry **I**n a large **R**eaction chamber; STAR: – **ST**irred **A**tmospheric flow **R**eactor). The details about its basic concept of operation have been described previously (Mentel et al., 2009; Baker et al., 2024). For this study the system was operated with a total flow rate of 60 L min^{-1}, of which 32 L min^{-1} were injected into the reactor, resulting in a residence time of approximately 60 min. Experimental conditions were maintained at 20 °C and at 20 % relative humidity. •OH radicals were produced by photolyzing hydrogen peroxide (H_2O_2) using two 254 nm UV-C lamps (TUV 16W 4P SE, Philips). The photolysis rate was controlled by reducing the photon flux by covering part of the lamps with adjustable bellows. H_2O_2 vapor was introduced into SAPHIR-STAR by bubbling a 0.2 L min^{-1} nitrogen (N_2) flow through a 30 % w/w H_2O_2 solution (Sigma-Aldrich).

In the α-pinene photooxidation experiments a continuous flow of 0.012 L min^{-1} from an α-pinene cylinder (with a concentration of $\sim$ 48.8 ppm) was injected into SAPHIR-STAR resulting in an initial concentration of $\sim$ 10 ppbv. For pinonaldehyde photooxidation, liquid pinonaldehyde (Orgentis chemicals, 99.7 %) was introduced by use of a syringe pump (Fusion 4000, Chemyx Inc.) at a flow rate of 0.145 µL h^{-1} resulting in a concentration of 5 ppbv of pinonaldehyde in the reactor. NO was injected into the chamber from a gas cylinder (20.09 ppm NO in N_2 5.0) via a mass flow controller for initial concentrations before reaction ranging between 0 and 7.5 ppbv.

To investigate the role of the H-abstraction pathway in α-pinene photooxidation we focused on the early stages of the reaction systems before secondary-generation products become important. All precursors were injected into the dark chamber. Once all precursors were well mixed and showed stable concentrations, the UV-C lamps were switched on for •OH production by photolysis. The UV-C lamps were then kept on at a constant setting for one hour to initialize the photooxidation of α-pinene, followed by three hours without irradiation to allow for products to be flushed out and for precursors to recover initial concentrations. This cycle was repeated three times for every system investigated.

Since the first hour of photooxidation is crucial for investigating the relative role of the H-abstraction channel compared to the •OH-addition channel, a cycle of one hour of photolysis followed by three hours without irradiation was repeated three times for each experimental condition listed in Table 1, as mentioned before. The time series of α-pinene, H_2O_2, and $C_{10}H_{17}O_7\bullet$ peroxy radicals over a total run of the experiments (14 h) are shown in Fig. S2, together with an example of the experimental procedure. During the final cycle the lamps were kept on continuously for 6 h to allow the system to reach steady state.

2.2 Methods and instrumentation

2.2.1 Instrumentation

The α-pinene concentration was measured by a proton-transfer-reaction mass spectrometry (PTR-TOF-MS, Ionicon Analytik GmbH). Gas concentrations of NO and NO_x were detected by a NO monitor (nCLD899, Eco Physics GmbH) coupled to a self-built photolytic NO_2 converter, with a detection limit of 0.05 ppb for NO measurement. O_3 was measured by O_3 monitor (O342e, Envea GmbH), with a detection limit of 0.2 ppb. H_2O was monitored by a Picarro CRDS analyzer (G2401, Picarro Inc.).

An Eisele type inlet (Eisele and Tanner, 1993) was coupled to an atmospheric-pressure-interference time-of-flight

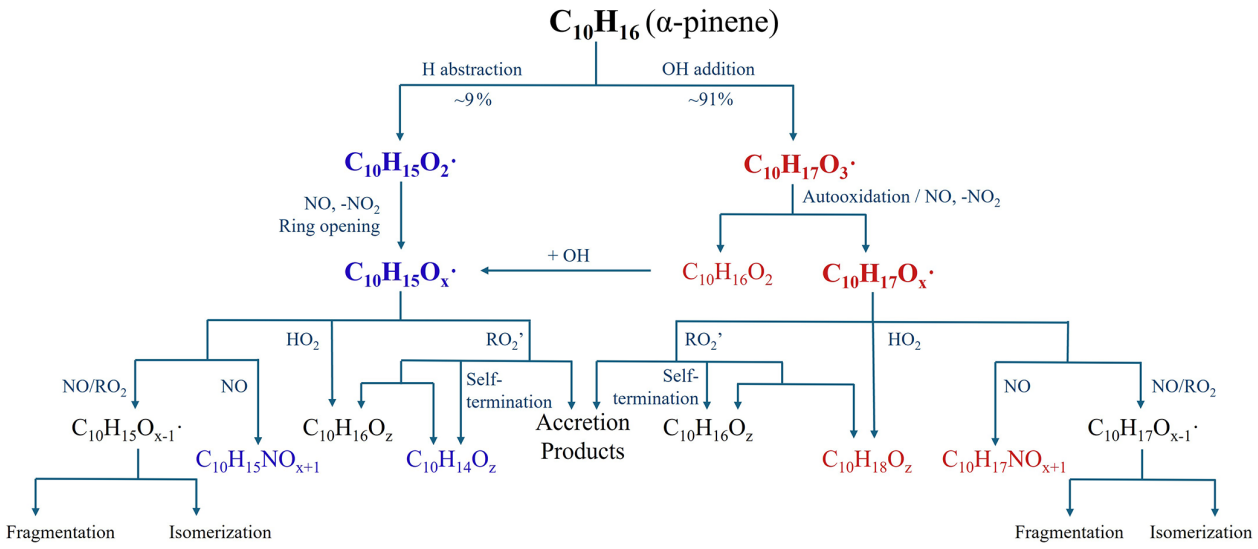

Figure 1. A schematic diagram illustrating •OH initiated α-pinene photooxidation through either the OH-addition pathway or the H-abstraction pathway. The unique peroxy radicals and their subsequent termination reactions are also depicted. The potential closure products are categorized into different families based on their formation pathways and the number of hydrogen atoms in molecules.

mass spectrometer (Api-TOF-MS, Tofwerk AG) using a positive reagent ion ($C_3H_7NH_3^+$) produced from propylamine ($C_3H_7NH_2$, $\geq 99\,\%$, Sigma Aldrich) to ionize less oxygenated organic products in gas phase (Berndt et al., 2018). The resolution of this instrument was ~ 3500 m/Δ m FWHM for m/z larger than 150. $C_3H_7NH_3^+$ has the advantage that it does cluster with pinonaldehyde very efficiently, which is vital for investigating α-pinene related systems since pinonaldehyde is a major oxidation product and a representative for the OH-addition pathway. The sensitivity of pinonaldehyde (Fig. S3) was calibrated in propylamine CIMS (amine-CIMS) by using a Liquid Calibration Unit (LCU, Ionicon Analytik GmbH). The long TOF-MS (LTOF, Tofwerk AG), with a resolution ~ 8500 m/Δ m FWHM for masses larger than 200 Th, was coupled with a multi-scheme ionization inlet (MION, Karsa Oy) (Rissanen et al., 2019). The MION inlet allows switching between bromide and nitrate modes, utilizing Br^- and NO_3^- as reagent ions, respectively. The Br^- was mainly used to detect HO_2• radicals and their relative change (Albrecht et al., 2019). NO_3^- CIMS has been shown to efficiently detect HOM (Ehn et al., 2014). Wang et al. have also shown that HOM(NO_3^-) clusters with four or more oxygen atoms in the HOM have a higher bonding strength than the H_2SO_4(NO_3^-) cluster (Wang et al., 2024), possibly due to the multiple hydroperoxyl and hydroxy functional groups present in HOM molecules (Bianchi et al., 2019). This indicates a relative sensitivity at the collision limit for these highly functionalized HOM. Since the study by Wang and coworkers (Wang et al., 2024) used the same setup regarding instrument and inlet we assumed that the MION-CIMS used in this study detects HOM compound with same sensitivity. All CIMS data were processed using the IGOR Pro (WaveMetrics) based Tofware v3.3.0.

2.2.2 •OH concentration, VOC turnover, and HO_2• concentration during steady stages

The concentration of •OH radicals was calculated based on the reacted fraction of α-pinene or pinonaldehyde under steady-state conditions (Eq. 1) (Kiendler-Scharr et al., 2009). When the system is in steady-state, all parameters are stable and injection rates equal loss rates. In Eq. (1), F represents the total flow through the chamber, and V is the volume of chamber. $[VOC]_0$ and $[VOC]_{SS}$ represent the VOC concentration in the dark and in steady state (SS), respectively. k_{OH} denotes the rate constants for the reaction of α-pinene or pinonaldehyde with •OH radicals, which are 5.4×10^{-11} cm^3 s^{-1} and 4.0×10^{-11} cm^3 s^{-1} at 20 °C, respectively (Atkinson and Arey, 2003; Rolletter et al., 2020). The estimated •OH concentrations are listed in Table 1. The turnover of VOC by •OH can be calculated using Eq. (2), which represents the amount of VOC consumed by the reaction with •OH (Baker et al., 2024).

$$[^{\bullet}OH]_{SS} = \frac{\frac{F}{V} \times \frac{[VOC]_0 - [VOC]_{ss}}{[VOC]_{ss}}}{k_{OH}} \quad (1)$$

$$\text{turnover}_{voc} = k_{OH} \times [VOC]_{SS} \times [^{\bullet}OH]_{SS} \quad (2)$$

To determine the concentrations of HO_2• in the chamber, a series of isoprene photooxidation experiments was conducted, and a corresponding box model based on the MCM v3.3.1 chemistry, which used the same boundary conditions, was applied. More details about the box model can be found in Baker et al. (2024).

In these experiments, a continuous flow of 0.050 L min^{-1} of isoprene from a gas cylinder (11.8 ± 0.24 ppmv, Linde GmbH) was introduced into the chamber to achieve a target concentration of 10 ppbv before reactions. The UV-C lamps were then adjusted in five different steps by varying the lamp bellows to vary $[\cdot OH]_{SS}$. The box model reproduced both $[isoprene]_{SS}$ and $[\cdot OH]_{SS}$ for each step within the measurement uncertainties (Fig. S4). A linear fit was applied to normalized $HO_2\cdot$ / $[Br^- + (H_2O)Br^-]$ (in normalized counts per second, ncps) and modelled $[HO_2\cdot]_{SS}$ (Fig. S5), and the slope was used as calibration factor for calculating $HO_2\cdot$ levels in subsequent experiments (Table 1).

2.2.3 Fuzzy *c*-means clustering (FCM)

Hierarchical clustering has been shown to be an effective dimensionality-reduction technique to identify major ion groups and patterns of chemical behaviour in mass spectrometry previously (Koss et al., 2020). Wu et al. demonstrated the application of the soft clustering method FCM for simplifying complex mass spectrometric data to reveal chemical and kinetic characteristics of chemical reaction systems (Wu et al., 2024). Here, FCM was applied to mass spectrometric data to explore the formation rates of a variety of products along competing reaction channels. The time series of 156 ions in the early reaction stage (up to 3000 s after start of the photooxidation processes) were selected for clustering. Herein, the major ions from both nitrate-CIMS and amine-CIMS were combined. Normalization was applied to all ions used since their typical time behaviour was more important for clustering than their absolute abundance. Initially, all ion signals were normalized relative to their corresponding reagent ions. Subsequently, Frobenius normalization was applied to each ion across the entire time range.

Three parameters were calculated to help to constrain the optimal number of clusters: sum of squared errors (SSE), distortions, and silhouette coefficient (Wu et al., 2024; Campello and Hruschka, 2006). The FCM algorithm was run 50 times for each cluster number in a range between 2 to 13. The results of the three parameters as function of cluster numbers are shown in Fig. S6. The four-cluster solution was then selected for the subsequent analysis.

2.2.4 Model simulations to determine early reaction stages

To clarify the role of the H-abstraction channel under various NO conditions, the early reaction stages are particularly relevant. In this study, we define early reaction stages using three criteria: (i) α-pinene turnover exceeds that of pinonaldehyde by a factor of ten, (ii) under conditions with NO, biomolecular reactions of $RO_2\cdot$ are dominated by $RO_2\cdot + NO$ and contribute more than 90 % to the biomolecular loss of $RO_2\cdot$, and (iii) α-pinene oxidation is primarily driven by •OH rather than O_3. Therefore, model simulations for α-pinene photooxidation systems were conducted to quantitively identify early reaction stages.

As shown in Fig. 2a-1 to c-1, the model captures the evolution of the system quite well but generally underestimates NO and O_3 concentrations. These discrepancies may arise from differences in the temporal resolution of measurements and simulations, physical effects introduced by the activation of the UV-C lamps (e.g., changing emissions due to temperature adjustment of the UV-C lamp), and uncertainties in the chemical mechanism including reactions currently not represented in the model framework. The $HO_2\cdot$ and $RO_2\cdot$ concentrations obtained from the simulations are shown in Fig. 2a-2 to c-2 together with the relative contributions of $RO_2\cdot + NO$, $RO_2\cdot + HO_2\cdot$ and $RO_2\cdot + NO$ to the total biomolecular $RO_2\cdot$ loss. Here, the reaction rates were calculated with $k_{[RO_2][HO_2]} = 1.85 \times 10^{-11}$ cm^3 s^{-1}, $k_{[RO_2][NO]} = 1 \times 10^{-11}$ cm^3 s^{-1} and $k_{[RO_2][RO_2]} = 5 \times 10^{-12}$ cm^3 s^{-1} (Baker et al., 2024; Berndt et al., 2016; Jenkin et al., 1997).

Based on these results, reactions occurring within the first 100, 100, and 320 s after initiation of reactions by starting the photooxidation were defined as early stages for the NO-free, low-NO, and high-NO conditions, respectively. The average bimolecular reaction rates for $RO_2\cdot + NO$ were negligible for cases without NO and increased to 0.179 and 1.06 s^{-1} for the low-NO and high-NO conditions, respectively. For $RO_2\cdot + HO_2\cdot$ reactions, the rates were 0.0055, 0.011, and 0.0075 s^{-1}, while those for $RO_2\cdot + RO_2\cdot$ reactions were 0.0075, 0.0029, and 0.0014 s^{-1} for NO-free, low-NO, and high-NO conditions, respectively. The contribution of $RO_2\cdot + NO$ was higher than 90 % under both low-NO and high-NO conditions.

For pinonaldehyde photooxidation under high-NO conditions, the reactions within the early reaction stages were also investigated to facilitate comparison with the corresponding α-pinene system under high NO conditions. Besides H-abstraction channel, reactions of α-pinene with O_3, and pinonaldehyde with •OH may also contribute to the formation of $C_{10}H_{15}O_x\cdot$ radicals. Therefore, the loss of α-pinene due to oxidation by O_3 formed as a byproduct of other reactions, and the loss of pinonaldehyde via •OH oxidation, were evaluated. The results are shown in detail in Fig. S7. In both cases, losses are smaller than 1 % of the reaction rate of α-pinene with •OH, which further supports our definition of early reaction stage being reasonable and representative.

3 Results and Discussion

3.1 $C_{10}H_{15}O_x\cdot$-related HOM form rapidly from α-pinene photooxidation in the presence of NO

All major products from α-pinene photooxidation that were detected by NO_3^- CIMS, in the absence or presence of NO, were categorized into the following groups: C_{10} monomers, C_{20} dimers, and $C_{<10}$ fragments. The time series for contri-

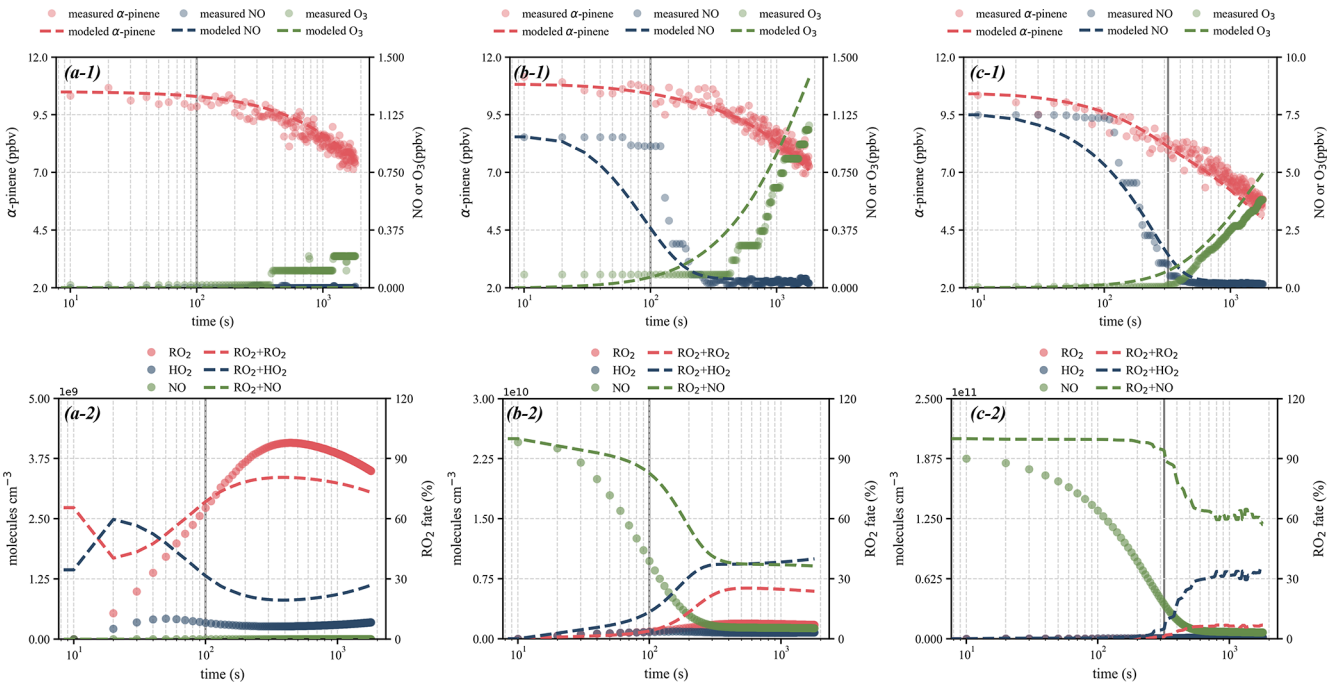

Figure 2. Results of model simulations for α-pinene photooxidation under NO-free **(a-1, a-2)**, low-NO **(b-1, b-2)**, and high-NO conditions **(c-1, c-2)**. The upper panels show modelled and measured concentrations of α-pinene, NO, and O_3 across the three conditions, while the lower panels show the corresponding radical concentrations of $RO_2\bullet$ and $HO_2\bullet$. In addition, the lower panels illustrate the relative contributions of $RO_2\bullet + HO_2\bullet$, $RO_2\bullet + RO_2\bullet$ and $RO_2\bullet + NO$ reactions to the total bimolecular reaction rate of $RO_2\bullet$ (shown as $RO_2\bullet$ fate on the right y-axis).

butions of each group varies for the three different NO conditions, as shown in Fig. 3a-1, a-2, a-3. A comparison under varying NO conditions is critical to elucidate the role of NO, since the presence of NO, ring opening and isomerization of alkoxy radicals, can be crucial in facilitating HOM formation from H-abstraction channel (Shen et al., 2022). The analysis was focused on the early reaction stages to explore the importance of the H-abstraction channel for HOM formation. The average product distributions of C_{10} monomers from early stage α-pinene photooxidation without and with NO are illustrated by Kendrik Mass Defect (KMD) plots as a function of oxygen number (Kendrick Mass = oxygen, Fig. 3b-1, b-2, b-3). Each plot features seven distinct families, with compounds in each family sharing the same carbon and hydrogen numbers but differing in oxygen content.

Under α-pinene NO-free conditions the relative contributions of $C_{10}H_{18}O_x$, $C_{10}H_{16}O_x$, and $C_{20}H_{34}O_x$ are 56.1 %, 11.1 %, and 8.8 %, respectively, and they are all closed-shell products related to $C_{10}H_{17}O_x\bullet$. The first generation peroxy radicals with four-membered ring-opening, $C_{10}H_{17}O_3\bullet$, can undergo fast unimolecular reactions with rates of $4 \pm 2\,s^{-1}$ (Xu et al., 2019). As shown in Fig. 3b-1, species with the formula $C_{10}H_{17}O_7\bullet$ are identified as predominantly HOM peroxy radicals and are detected in the nitrate mass spectra as $C_{10}H_{17}O_7(NO_3^-)$. This agrees with previous observations by Berndt (2021), which were obtained using four different reagent ions, and calculations by Piletic and Kleindienst (2022). Additional $HO_2\bullet$ radicals were produced in our experiments via the reaction of the •OH radical with H_2O_2. The increasing contribution of $C_{10}H_{18}O_x$ (Fig. 3(1-a)) indicates a significant termination reaction of $RO_2\bullet$ by $HO_2\bullet$. Among the $C_{10}H_{18}O_x$ family, $C_{10}H_{18}O_7$ shows the highest intensity and is likely produced via termination reactions of $C_{10}H_{17}O_7\bullet$ with $HO_2\bullet$, which aligns with the dominance of $C_{10}H_{17}O_7\bullet$ in the $C_{10}H_{17}O_x\bullet$ family. Compounds with six oxygen atoms but one hydrogen less or one more hydrogen than $C_{10}H_{17}O_7\bullet$ (i.e., $C_{10}H_{16}O_6$ and $C_{10}H_{18}O_6$) are significant contributors to the total product signal of the $C_{10}H_{17}O_x\bullet$ family. Compounds with the formula $C_{10}H_{16}O_6$ likely have carbonyl functionalities and are formed either directly from Reaction (R3) or from self-termination reactions of $C_{10}H_{17}O_7\bullet$ (Reaction R8) (Iyer et al., 2018; Jenkin et al., 2019). In contrast, $C_{10}H_{18}O_6$ species are possibly alcohols formed from $C_{10}H_{17}O_7\bullet$ via Reaction (R3), or more likely hydroperoxides derived from $C_{10}H_{17}O_6\bullet$ via Reaction (R1) (Iyer et al., 2018; Jenkin et al., 2019).

In addition to C_{10} HOM monomers, C_{20} accretion products also significantly contribute to HOM, particularly species containing 8, 10, or 12 oxygen atoms (Fig. S8). These have been identified as the most abundant dimers from •OH initiated α-pinene photooxidation system by Berndt et al. (2016). $C_{20}H_{34}O_{(8,10,12)}$ can be mechanis-

Table 1. Overview of experimental conditions: pinonaldehyde photooxidation without NO (NO-free) and with high NO (high-NO), α-pinene photooxidation without NO (NO-free), with low NO (low-NO), and with high NO (high-NO). The precursor concentrations in the dark and in photooxidation steady-state conditions are shown at t_0 and t_S, respectively. The measurement uncertainty is less than 5 %. Details about how to estimate •OH and HO_2• radicals are given in Sect. 2.2.

		VOC		NO (ppbv)	•OH (# cm^{-3})	HO_2• (# cm^{-3})
		pinonaldehyde (ppbv)	α-pinene (ppbv)			
Pinonaldehyde (NO-free)	t_0	1.5	–	0	–	–
	t_S	0.75	–	0	6.5×10^6	6.4×10^8
Pinonaldehyde (high-NO)	t_0	1.8	–	7.0 ± 0.13	–	–
	t_S	0.75	–	0.36 ± 0.01	9.3×10^6	2.7×10^8
α-pinene (NO-free)	t_0	–	10.3 ± 1.7	0	–	–
	t_S	0.01	8.3 ± 1.4	0	1.25×10^6	3.1×10^8
α-pinene (low-NO)	t_0	–	11.1 ± 1.3	0.91 ± 0.05	–	–
	t_S	0.05	5.5 ± 1.7	0.05 ± 0.01	5.1×10^6	9.8×10^8
α-pinene (high-NO)	t_0	–	10.6 ± 1.3	7.4 ± 0.05	–	–
	t_S	0.09	4.2 ± 2.1	0.16 ± 0.01	7.5×10^6	1.0×10^9

tically explained by recombination of $C_{10}H_{17}O_7$• with $C_{10}H_{17}O_3$•, $C_{10}H_{17}O_5$•, or another $C_{10}H_{17}O_7$• via Reaction (4). $C_{10}H_{17}O_{(3,5,7)}$• have previously been reported to dominate the product spectrum (Lee et al., 2023; Berndt, 2021). In summary, the obtained HOM distributions in the base case without NO addition are consistent with previous studies and show mechanistically reasonable results.

When reactions are initiated in the presence of NO, the product distribution in the early reaction stage (when the RO_2• + NO regime is dominant) differs significantly from the NO-free case. The $C_{10}H_{17}NO_x$ product family, identified as organic nitrates, accounts for 29.9 % and 29.4 % of the total signal under low-NO and high-NO conditions, respectively, and dominates $C_{10}H_{17}O_x$•-related HOM families. The most abundant species with formulas $C_{10}H_{17}NO_{(6,7,8)}$ most likely represent organic nitrates formed via reactions of $C_{10}H_{17}O_{(5,6,7)}$• with NO. As the initial NO concentration increases, contribution from $C_{10}H_{17}O_6$•-derived HOM, such as $C_{10}H_{17}NO_7$ and $C_{10}H_{18}O_6$, also rises (Figure S9). When the initial NO increased from 0.91 ± 0.05 to 7.4 ± 0.05 ppbv, the ratios of $C_{10}H_{17}NO_7$ to $C_{10}H_{17}NO_8$ and $C_{10}H_{18}O_6$ to $C_{10}H_{18}O_7$ are enhanced from 0.32 to 0.43 and from 0.63 to 0.78, respectively. At least one alkoxy step (Reaction R7) is necessary to produce peroxy radicals with even number, e.g. $C_{10}H_{17}O_6$•. Therefore, the presence NO promotes the occurrence of alkoxy steps in HOM formation. Compared to the NO-free condition, the contributions of accretion products with $C_{20}H_{34}O_{(9,11)}$ are also promoted. For forming $C_{20}H_{34}O_{(9,11)}$ via Reaction (R5) an $C_{10}H_{17}O_x$• peroxy radical with an even oxygen number must be involved, e.g. $C_{10}H_{17}O_4$• and $C_{10}H_{17}O_6$•, further highlighting the role of alkoxy steps in HOM formation.

The $C_{10}H_{17}O_7$• peroxy radicals exhibit a rapid formation rate and a high molar yield in α-pinene photooxidation systems, but their formation shows only a weak dependence on the NO concentration. Although •OH addition to α-pinene yields three structural first-generation isomers ($C_{10}H_{17}O_3$•), only the isomer that undergoes an opening of the four-membered ring is capable of subsequent autoxidation (Lee et al., 2023; Piletic and Kleindienst, 2022; Berndt et al., 2016). The ring-opened $C_{10}H_{17}O_3$• can then undergo two rapid unimolecular autoxidation steps, with a rate constant of approximately 4 s^{-1} for the first step which will lead to the formation of $C_{10}H_{17}O_5$•, and a rate constant around 10 s^{-1} for the subsequent step and formation of $C_{10}H_{17}O_7$• species (Piletic and Kleindienst, 2022; Xu et al., 2019). The fast autoxidation steps of the resulting peroxy radicals imply that the characteristic timescales of their formation are significantly shorter than those of competing bimolecular reactions with NO, RO_2•, and HO_2•, whose maximum effective rates in our experiments range from 0.02 to 1.88 s^{-1} under NO-free, low-NO, and high-NO conditions, respectively. Therefore, biomolecular reactions, particularly involving NO, cannot effectively compete with the rapid autoxidation reactions, which can explain the observed weak NO dependence of the formation of $C_{10}H_{17}O_7$•-related HOM.

In addition to the change of $C_{10}H_{17}O_x$•-related HOM, $C_{10}H_{15}O_x$•-related HOM families emerge once NO is introduced into the system (Fig. 3a-2, a-3, b-2, b-3). Under the NO-free condition, neither the $C_{10}H_{15}NO_x$ nor the $C_{10}H_{14}O_x$ family contributes more than 2 %. However, under low-NO conditions their contribution rises to 10.3 % and 4.7 %, respectively, and further increases to 24.9 % and 6.0 % under high-NO conditions. The most abundant peroxy radical in $C_{10}H_{15}O_x$• family is $C_{10}H_{15}O_7$•, as shown in Fig. S9,

followed by $C_{10}H_{15}O_9\bullet$, which is consistent with the closed shell organic nitrate distribution, where $C_{10}H_{15}NO_8$ is most prevalent, followed by $C_{10}H_{15}NO_{10}$. The $C_{10}H_{14}O_x$ family contains products with carbonyl groups and is formed via self-termination reactions of peroxy radicals. In addition to C_{10} monomers, accretion products with the formula $C_{20}H_{30}O_x$ and $C_{20}H_{32}O_x$, derived from Reaction (R5), also increase with elevated NO concentrations. Here at least one peroxy radical containing 15 hydrogen atoms must be involved (Berndt et al., 2018). Compared to monomers, formation of accretion products is reduced since in early stages of the reactions the $RO_2\bullet + R'O_2\bullet$ pathway is less important compared to the NO + $RO_2\bullet$ pathway or the $RO_2\bullet$ autoxidation. The intensity of $C_{10}H_{16}O_7$ increases gradually until it surpasses that of $C_{10}H_{16}O_6$, which in the absence of NO is the most abundant peak. $C_{10}H_{16}O_7$ is likely a carbonyl compound (or family), formed either through Reaction (R3), or from self-termination. Both need $C_{10}H_{17}O_8\bullet$ as precursors. However, analysis of the closed-shell families $C_{10}H_{18}O_x$ and $C_{10}H_{17}NO_x$ indicates the absence of significant formation of $C_{10}H_{17}O_8\bullet$ in presence of NO, which also aligns with Berndt (2021) and Piletic and Kleindienst (2022). $C_{10}H_{16}O_7$ may also be a hydroperoxide produced via Reaction (R2), or an alcohol produced via Reaction (R3), with $C_{10}H_{15}O_7\bullet$ peroxy radicals or $C_{10}H_{15}O_8\bullet$ peroxy radicals serving as precursors. Products formed via $RO_2\bullet + RO_2\bullet$ reactions were produced at significantly slower rates than other species, as will be discussed in Sect. 3.2. Additionally, when $C_{10}H_{15}O_7\bullet$ reacts with another $RO_2\bullet$ radical, it forms $C_{10}H_{16}O_6$ or $C_{10}H_{14}O_6$ rather than $C_{10}H_{16}O_7$. Thus, Reaction (R3) was considered to not contribute significantly, and the reaction of $C_{10}H_{15}O_7\bullet$ with $HO_2\bullet$ most likely accounts for the significant increase of $C_{10}H_{16}O_7$. Similarly, species in the $C_{10}H_{16}O_x$ family that have more than seven oxygen atoms can be attributed to reactions of $C_{10}H_{15}O_x\bullet$ peroxy radicals with $HO_2\bullet$.

Contributions from peroxy radicals containing more than seven oxygen atoms to the $C_{10}H_{17}O_x\bullet$ family are negligible, which is consistent with the number of oxygen atoms in the observed closed-shell products. This phenomenon is in accordance with previous measurement studies and calculations (Berndt, 2021; Lee et al., 2023). In the NO-free condition, compounds with more than seven oxygen atoms account for only 0.1 % of the $C_{10}H_{18}O_x$ family, whereas for the low-NO and high-NO cases, compounds with more than eight oxygen atoms contribute 5 % and 6 %, respectively, to the $C_{10}H_{17}NO_x$ family. Although the fate of the $C_{10}H_{17}O_7\bullet$ family remains unclear, the product distributions indicate that it is unlikely for them to undergo further steps of autoxidation. However, the $C_{10}H_{15}O_x\bullet$-related HOM are more oxidized than $C_{10}H_{17}O_x\bullet$-related HOM. For example, species containing more than eight oxygen atoms in $C_{10}H_{15}NO_x$ account for 43.6 % and 46.7 % in low-NO and high-NO cases, respectively, of the entire $C_{10}H_{15}NO_x$ family. Obviously $C_{10}H_{15}O_x\bullet$ isomers with $x \geq 7$ are formed, which exhibit faster unimolecular reaction rates than the accessible isomers of the $C_{10}H_{17}O_x\bullet$ peroxy radicals.

The distribution of the less oxygenated compounds was investigated based on the mass spectra detected by amine-CIMS, which are shown in Fig. S10. Consistent with nitrate-CIMS, $C_{10}H_{15}O_x\bullet$-related less oxygenated compounds also emerge with elevated NO concentrations, particularly those in the $C_{10}H_{14}O_x$ and $C_{10}H_{15}NO_x$ families. The dominant compounds in the $C_{10}H_{15}NO_x$ family are $C_{10}H_{15}NO_4$, $C_{10}H_{15}NO_6$, and $C_{10}H_{15}NO_8$, which should be derived from Reaction (R6) involving peroxy radicals with the formula $C_{10}H_{15}O_3\bullet$, $C_{10}H_{15}O_5\bullet$, and $C_{10}H_{15}O_7\bullet$, respectively. Among the major compounds in the $C_{10}H_{15}NO_x$ family detected by amine-CIMS only highly oxidized species with the formular $C_{10}H_{15}NO_8$ can also be detected in significant amounts by nitrate-CIMS. The same phenomenon can also be seen for $C_{10}H_{17}O_x\bullet$-related compounds. In amine-CIMS, the first-generation peroxy radical, $C_{10}H_{17}O_3\bullet$, and its associated closed-shell products play a dominant role in the combined $C_{10}H_{17}O_x\bullet$, $C_{10}H_{18}O_x$, and $C_{10}H_{17}NO_x$ families, although the $C_{10}H_{17}O_7\bullet$ related products are dominant in the mass spectrum obtained by nitrate-CIMS. For example, $C_{10}H_{17}NO_4$ and $C_{10}H_{18}O_3$ are major peaks, which are produced mechanistically through termination reactions of $C_{10}H_{17}O_3\bullet$ by NO and by $HO_2\bullet$ radicals, respectively. $C_{10}H_{17}NO_4$ contributes 56.6 % and 57.5 % to the $C_{10}H_{17}NO_x$ family in low-NOand high-NO conditions, respectively. $C_{10}H_{18}O_3$accounts for 70.6 %, 77.6 %, and 69.3 % in NO-free, low-NO, and high-NO cases, respectively.

Only ring-opened $C_{10}H_{17}O_3\bullet$ can undergo fast autoxidation reactions to produce HOM, and they account only for approximately 25 % of the sum of $C_{10}H_{17}O_3\bullet$ peroxy radicals derived from the •OH addition pathway (Xu et al., 2019, Vereecken et al., 2007). However, the nitrate-CIMS technique ionizes specifically highly oxygenated organics (Ehn et al., 2014), resulting in the detection of only a narrow range of highly oxidized compounds derived from four-membered ring-opened $C_{10}H_{17}O_3\bullet$. The amine-CIMS is efficient in detecting a large range of products including less oxygenated compounds ($O < 7$) (Berndt, 2021). $C_{10}H_{16}O_2(C_3H_7NH_3^+)$ is found to be the strongest peak among the entire mass spectrum in amine-CIMS, indicating the production of pinonaldehyde. Pinonaldehyde can be formed from the formation of alkoxy radicals via reactions of four-membered ring-retained $C_{10}H_{17}O_3\bullet$ peroxy radicals and NO, which then undergo a fast opening of the six-membered ring, shown in Fig. S1 (Rolletter et al., 2019). The inclusion of amine-CIMS extends the detection of products, especially less oxygenated ones, which could indicate the fate of four-membered ring-retained $C_{10}H_{17}O_3\bullet$ peroxy radicals.

Alkoxy radicals derived from reactions involving $C_{10}H_{17}O_x\bullet$ peroxy radicals and NO can undergo an H-shift, β-scissions, or a $HO_2\bullet$ loss step; however, none of these reactions are expected to form $C_{10}H_{15}O_x\bullet$ peroxy radicals

directly. For example, neither H-migration nor β-scission will lead to the loss of a hydrogen atom without a carbon-carbon bond cleavage, and the resulting alkyl radicals will react efficiently with O_2 to regenerate $C_{10}H_{17}O_x\bullet$ radicals and thus continue the autooxidation cycle. The $HO_2\bullet$ loss channel is expected to be a minor pathway for the considered alkoxy radicals, because intramolecular H-migration and β-scission are more favorable, as previously shown by Vereecken and Peeters (2009, 2010). If the $HO_2\bullet$ loss channel would happen, it would lead to the formation of carbonyl and $HO_2\bullet$, losing one hydrogen atom forming $C_{10}H_{16}O_x$ products. While the $C_{10}H_{16}O_x$ products could, in principle, react with •OH radical again to produce $C_{10}H_{15}O_x\bullet$ intermediates, this process would occur on the timescale of secondary chemistry and is therefore unlikely to contribute significantly during the early reaction stages. Pinonaldehyde was dominant among $C_{10}H_{16}O_x$ compounds, but its oxidation cannot become a significant source of $C_{10}H_{15}O_x\bullet$-related HOM, which will be discussed in Sect. 3.2.

In conclusion, the product distributions from α-pinene photooxidation during early reaction stages were investigated. Compared to NO-free conditions, the presence of NO enhanced the formation of organic nitrates and promoted alkoxy formation steps, which lead to significant formation of $C_{10}H_{15}O_x\bullet$-related compounds. These were detected by both nitrate-CIMS and amine-CIMS. The initial peroxy radicals leading to $C_{10}H_{15}O_x\bullet$ related products were identified as $C_{10}H_{15}O_3\bullet$, which cannot arise from ozonolysis of α-pinene since α-pinene was dominantly oxidized by •OH radicals rather than O_3, as shown in Fig. S7. Also, $C_{10}H_{15}O_4\bullet$ peroxy radicals are mechanistically expected to be first generation peroxy radicals in ozonolysis. Potential mechanisms that could be responsible for the emergence of $C_{10}H_{15}O_x\bullet$-related HOM will be discussed in the following section.

3.2 $C_{10}H_{15}O_x\bullet$-related HOM attributed to H-abstraction pathway

In α-pinene oxidation systems three possible pathways can lead to monomers with 15 hydrogen atoms: either the H-abstraction channel by •OH radicals (Shen et al., 2022) , ozonolysis (Berndt, 2022), or oxidation of pinonaldehyde (Rolletter et al., 2020). However, as mentioned in Sects. 2.2 and 3.1, ozone was not present at the beginning of each transient cycle and accounted for less than 1 % of α-pinene reaction loss. Thus ozonolysis cannot explain the significant formation of $C_{10}H_{15}O_x\bullet$-related products, in particular •OH-initiation yields more HOM than ozonolysis (Berndt, 2022). To explore potential formation pathways of $C_{10}H_{15}O_x\bullet$-related compounds, FCM clustering was applied to the time series of 156 ions detected by nitrate-CIMS and amine-CIMS. Selection criteria for the ions were contributions of more than 0.1 % to the total ion signal in nitrate-CIMS or more than 1 % to the total ion signal in amine-CIMS.

A four-cluster solution was identified as the optimal solution. Corresponding results are presented in Fig. 4. Figure 4a shows the time series of the four cluster centers and the contributing ions. Compounds in cluster 1 form immediately after reactions are initiated by switching on the UV-C lamps, followed by cluster 2 and cluster 3, while compounds in cluster 4 show the longest formation time. The cluster centers peak at approximately 160, 210, 290, and 850 s, respectively. As shown in Fig. 4b, the major monomers in the $C_{10}H_{18}O_x$ family and the major dimers ($C_{20}H_{30}O_x$, $C_{20}H_{32}H_{12}$, $C_{20}H_{34}O_8$) are all found in cluster 4, which exhibits the slowest formation rate among four clusters. These compounds originate from biomolecular termination reactions (Reactions R1 and R5), with their production rates largely controlled by the concentration of $HO_2\bullet$ and $RO_2\bullet$ radicals. NO is already in a steady state in the dark chamber, while $HO_2\bullet$ and $RO_2\bullet$ only begin to accumulate after the UV-C lamps are switched on. Therefore, the $RO_2\bullet$ fate is immediately affected by NO. Consequently, under high-NO conditions, $RO_2\bullet$ + NO reactions as well as autoxidation play a dominant role for the $RO_2\bullet$ in early reactions, and only these two reactions are discussed in following sections.

Compounds in cluster 1 and cluster 2 initially increase dramatically before decreasing again, and cluster 1 exhibits a steeper decline than cluster 2. The bulk chemical properties and the average carbon oxidation state ($\overline{OSc}$) of each cluster are calculated (Kroll et al., 2011; Wu et al., 2021) and plotted as a function of average carbon (n_C) or nitrogen atoms (n_N) (Fig. S11). The early-generation cluster 1 exhibits the highest $\overline{OSc}$ and n_N but the lowest n_C, indicating that it mainly consists of highly oxidized nitrogen-containing compounds and fragments ($C < 10$). This characteristic distinguishes cluster 1 from the other clusters. It is determined by the emerging of •OH radicals at elevated NO concentration in the early stage.

The formation rate of each cluster can be interpreted kinetically as "typical" chemical formation rate (Wu et al., 2024). The compounds $C_{10}H_{15}NO_7(NO_3^-)$ and $C_{10}H_{15}NO_8(NO_3^-)$ are assigned to cluster 1 with the fastest formation rate; thus, they are likely first-generation products. Pinonaldehyde ($C_{10}H_{16}O_2(C_3H_7NH_3^+)$), a possible precursor, can only be found in cluster 3, which has a much slower formation rate. This clearly shows that pinonaldehyde oxidation cannot explain the production of $C_{10}H_{15}NO_7(NO_3^-)$ or $C_{10}H_{15}NO_8(NO_3^-)$. $C_7H_9NO_8(NO_3^-)$, which is detected in high amount in nitrate-CIMS and also attributed to cluster 1, goes through a fragmentation step and is possibly formed via decomposition of $C_{10}H_{15}O_x\bullet$, followed by further autoxidation and termination reactions by NO (Shen et al., 2022). Therefore, H-abstraction is probably the reason for the significant formation of $C_{10}H_{15}O_x\bullet$-related HOM, and not the oxidation of pinonaldehyde. The fragment $C_7H_{11}NO_8(NO_3^-)$ is formed faster than the organic nitrate monomer $C_{10}H_{17}NO_8(NO_3^-)$, even though both are initialized by the OH-addition channel. This relation differs from that of $C_7H_9NO_8(NO_3^-)$ and $C_{10}H_{15}NO_8(NO_3^-)$.

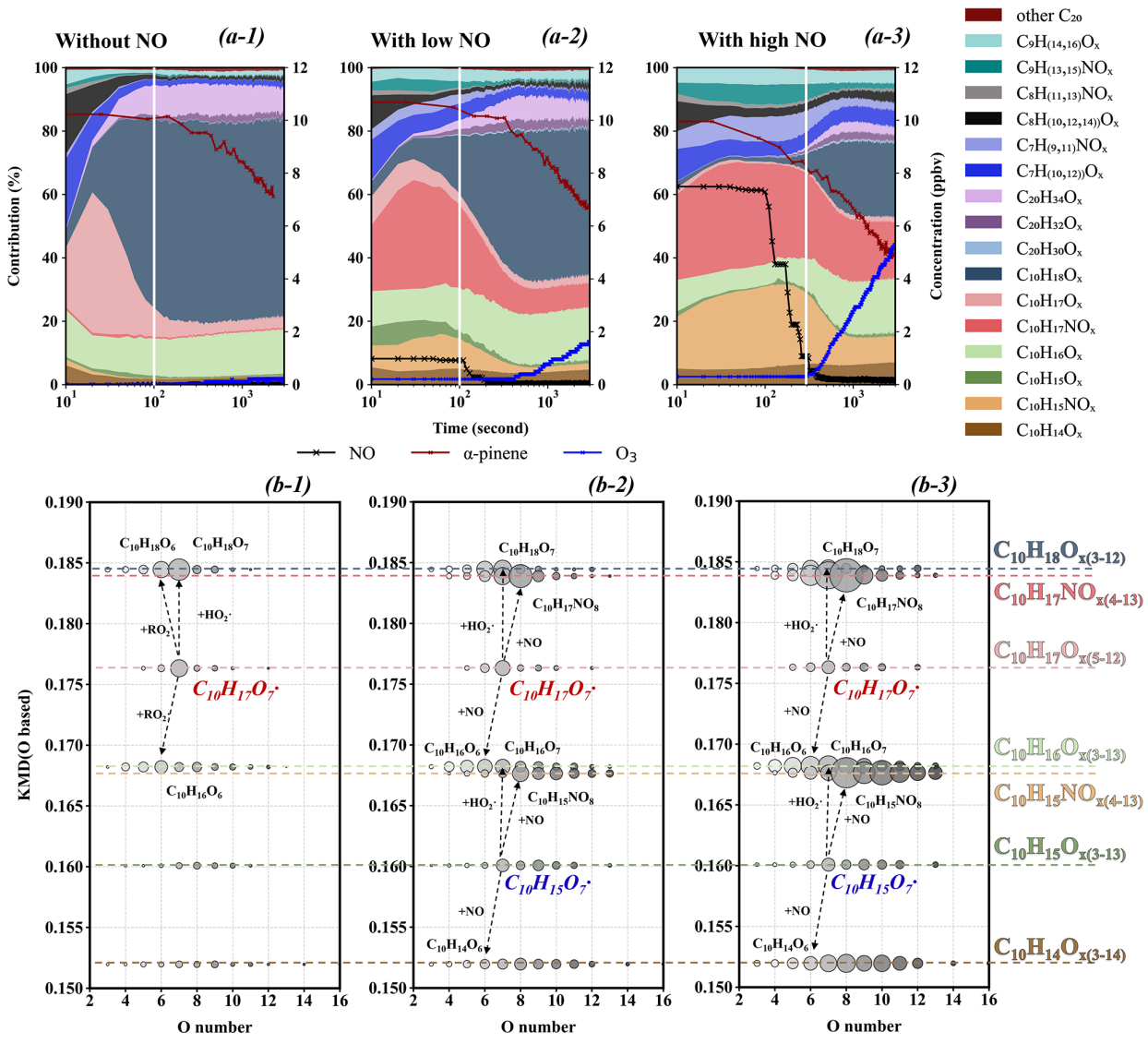

Figure 3. Panels **(a-1)**, **(a-2)**, **(a-3)** show stacked figures with the contributions of each product family from α-pinene photooxidation as a function of reaction time. The families representing major monomers (C = 10), fragments (C < 10), and accretion products (C = 20) are included in panels (a-1, a-2, a-3). Time series of concentrations for α-pinene, NO, and O_3 are also presented. The corresponding panels **(b-1)**, **(b-2)**, **(b-3)** located below each stack plot show the Kendrik Mass Defect (KMD, based on oxygen weight) of monomer compounds as a function of oxygen number, with marker sizes indicating the relative abundance of each compound in the early reaction stages (0–100, 0–100, and 0–320 s after reaction starts for **(b-1)**, **(b-2)**, and **(b-3)**, respectively. This is also indicated by the vertical white lines in **(a-1)**, **(a-2)**, and **(a-3)**). Compounds aligned along the same horizontal dashed lines are in same family, with the same carbon and hydrogen number but differing in oxygen number. Family names are shown on the right. The texts in panels **(b-1)**, **(b-2)**, **(b-3)** highlight major compounds with high abundance and their possible formation pathways. NO conditions increase in the panels from left to right, from NO-free and low-NO to high-NO, respectively. The products here are detected by nitrate-CIMS.

As shown in Fig. S12, the summed abundance of C_7 families ($C_7H_{(10,12)}O_x$, $C_7H_{(9,11)}NO_x$) increases accordingly with the increase of the NO injection, accounting for 0.01 %, 0.3 % and 2.4 % of HOM compounds under NO-free, low-NO and high-NO conditions, respectively. It indicates increasing alkoxy radical decomposition with increasing NO. C_7 fragments are formed via dissociation of C_{10} alkoxy radicals derived from bimolecular reactions of C_{10} peroxy radicals with NO. Thus, the presence of NO promotes C_7 fragments by enhancing the production of alkoxy radicals (Vereecken and Peeters, 2000; Berndt, 2021). The most abundant families, $C_7H_9NO_x$ and $C_7H_{11}NO_x$, likely originate from decomposition of $C_{10}H_{15}O_{x-1}$• and $C_{10}H_{17}O_{x-1}$•, respectively. Under high-NO conditions, the ratio of $C_7H_9NO_x$

to $C_{10}H_{15}NO_x$ reaches 0.22, substantially higher than the ratio of $C_7H_{11}NO_x$ to $C_{10}H_{17}NO_x$ (0.05). This observation suggests that either alkoxy radical formation or subsequent decomposition is more efficient in the H-abstraction pathway than in the •OH-addition pathway.

Evidence for alkoxy radical H-migration is provided by the enhanced formation of $C_{10}H_{17}NO_7$ and $C_{20}H_{34}O_{11}$ under high-NO conditions (Fig. S9). According to the oxygen-parity framework, $C_{10}H_{17}O_x$• radicals formed solely through autoxidation are expected to contain an odd number of oxygen atoms, whereas an alkoxy H-migration step changes the oxygen parity from odd to even (Kang et al., 2025). Thus, the observed increase in $C_{10}H_{17}NO_7$ and $C_{20}H_{34}O_{11}$ suggests the formation of $C_{10}H_{17}O_6$• peroxy radicals through at least one alkoxy radical isomerization step.

To initialize the HOM chain via •OH-addition pathway, four-membered rings must open from chemically activated tertiary radicals, which is independent of NO (Xu et al., 2019). In contrast, HOM formation through the H-abstraction pathway requires NO. The initially formed peroxy radicals ($C_{10}H_{15}O_2$•) are unlikely to undergo autoxidation directly; therefore, their reaction with NO to form alkoxy radicals ($C_{10}H_{15}O$•), followed by the ring-opening step producing $C_{10}H_{15}O_3$• radicals, is necessary to initiate the HOM formation chain.

As autoxidation proceeds, higher oxygenated peroxy radicals, such as $C_{10}H_{17}O_x$• and $C_{10}H_{15}O_x$•, are formed from $C_{10}H_{17}O_3$• and $C_{10}H_{15}O_4$•, respectively. These peroxy radicals can further react with NO, yielding either the corresponding alkoxy radicals ($C_{10}H_{17}O_{x-1}$• and $C_{10}H_{15}O_{x-1}$•) or organic nitrates ($C_{10}H_{17}NO_{x+1}$ and $C_{10}H_{15}NO_{x+1}$). However, the branching ratio between these two channels remains poorly constrained, contributing substantial uncertainty to the role of NO in HOM formation. Once formed, the fate of alkoxy radicals strongly depends on alkoxy radical structure (Vereecken and Peeters, 2010, 2009). Regardless of whether the precursor RO_2• radicals originate from the •OH-addition or H-abstraction pathway, their subsequent chemistry can proceed through alkoxy radical intermediates. Therefore, the fate of these alkoxy radicals ultimately determines the impact of NO on HOM formation.

Overall, NO does influence HOM formation through alkoxy-radical chemistry. By promoting the conversion of RO_2• radicals to RO• radicals, NO initializes pathways for H-migration and decomposition that would otherwise be less important. The extent to which these processes enhance or suppress HOM formation depends strongly on the structures of both the peroxy and alkoxy radicals, introducing substantial uncertainty into the overall role of NO.

To assess the robustness of the clustering results, additional cluster analysis was performed using a three- and five-cluster solution, as shown in Figs. S13 and S14, respectively. Consistent conclusions are obtained regardless of the number of clusters specified. In particular, the key compounds derived from the H-abstraction channel, such as $C_{10}H_{15}NO_8(NO_3^-)$ and $C_7H_9NO_8(NO_3^-)$, were consistently assigned to the first cluster with the fastest formation rate. The stability of the clustering results was further evaluated by performing 50 clustering runs with random initializations and using the four-cluster solution. The distributions of the cluster assignments were then analysed, as shown in Fig. S15, with particular attention given to the key compounds discussed above, including $C_{10}H_{15}NO_8(NO_3^-)$, $C_7H_9NO_8(NO_3^-)$, and $C_{10}H_{16}O_2(C_3H_7NH_3^+)$. The results demonstrate the high stability of the cluster solution, as these compounds were consistently assigned to the same cluster across all runs. For example, $C_{10}H_{15}NO_8(NO_3^-)$ was assigned to the first cluster in all runs. Therefore, the clustering results and insights derived from them are highly robust and reliable.

To assess the potential contribution of pinonaldehyde oxidation to the formation of $C_{10}H_{15}O_x$•-related HOM, pinonaldehyde photooxidation experiments were conducted under NO-free and high-NO conditions, analogous to conditions applied in the α-pinene systems (Table 1). Time series of α-pinene and its oxidation product pinonaldehyde during the first 30 min of the α-pinene (high-NO) experiment are shown in Fig. 5a-1. The corresponding turnovers of α-pinene and pinonaldehyde are presented in Fig. 5a-1. Similarly, the concentration of pinonaldehyde and its turnover during the pinonaldehyde (high-NO) experiment are shown in Fig. 5a-2. •OH concentrations were estimated using model simulations.

During the early stage, the average pinonaldehyde turnover was 8.9×10^6 molecules cm^{-3} s^{-1} under pinonaldehyde (high-NO) condition, approximately 6 times higher than the turnover (1.5×10^6 molecules cm^{-3} s^{-1}) under α-pinene (high-NO) condition. To facilitate comparison between the two experiments, we calculated the pinonaldehyde turnover for both experiments and compared it to obtain the ratio between the α-pinene (high-NO) and pinonaldehyde (high-NO) experiments (hereafter referred to as the pinonaldehyde turnover ratio). Signals measured in the pinonaldehyde experiment were subsequently normalized by this ratio to account for differences in the pinonaldehyde turnover between the two systems. The distributions of major $C_{10}H_{15}O_x$•-related products observed during α-pinene and pinonaldehyde experiments are presented in Fig. 5b. Major products belonging to the $C_{10}H_{14}O_x$ and $C_{10}H_{15}NO_x$ family detected by both nitrate-CIMS (N) and amine-CIMS (A) are included. The data shown in Fig. 5b represents averages over the first 320 s following the initiation of oxidation, corresponding to the early reaction stage, during which RO_2• + NO accounts for more than 90 % of the total bimolecular RO_2• loss rate. In addition, all product signals here as well as all data used for comparison in the following paragraphs have been normalized by the pinonaldehyde turnover.

The pinonaldehyde turnover ratio during the first 320 s exceeded 5 and was substantially higher during the first 100 s. This large difference arose because pinonaldehyde was present at the start of the pinonaldehyde system and was

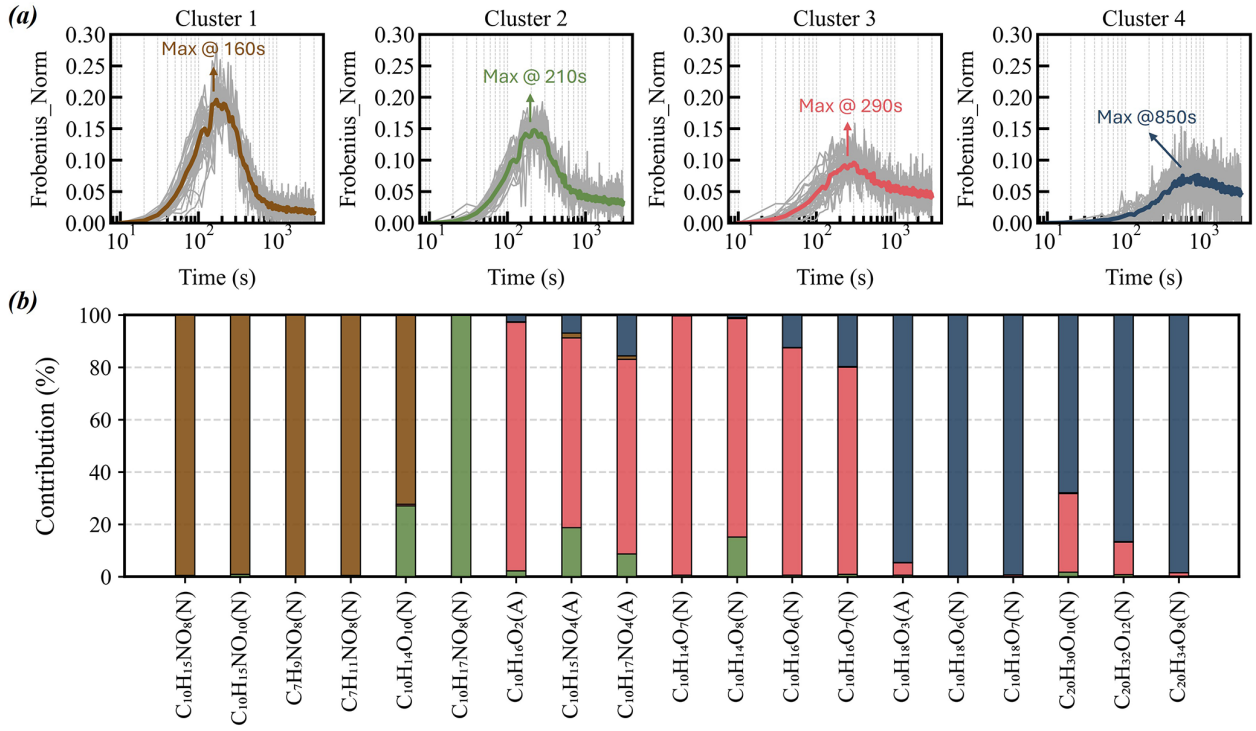

Figure 4. Results of fuzzy *c*-means clustering for the dominant peaks (156 in total) during early reaction stages of α-pinene photooxidation under high NO condition are shown in panel **(a)**. The four-cluster solution is shown here. The time series of the cluster centers are displayed as colored solid lines, while individual species are shown in gray lines. Panel **(b)** illustrates the cluster apportionment of selected major products detected in both nitrated-CIMS (N) and amine-CIMS (A).

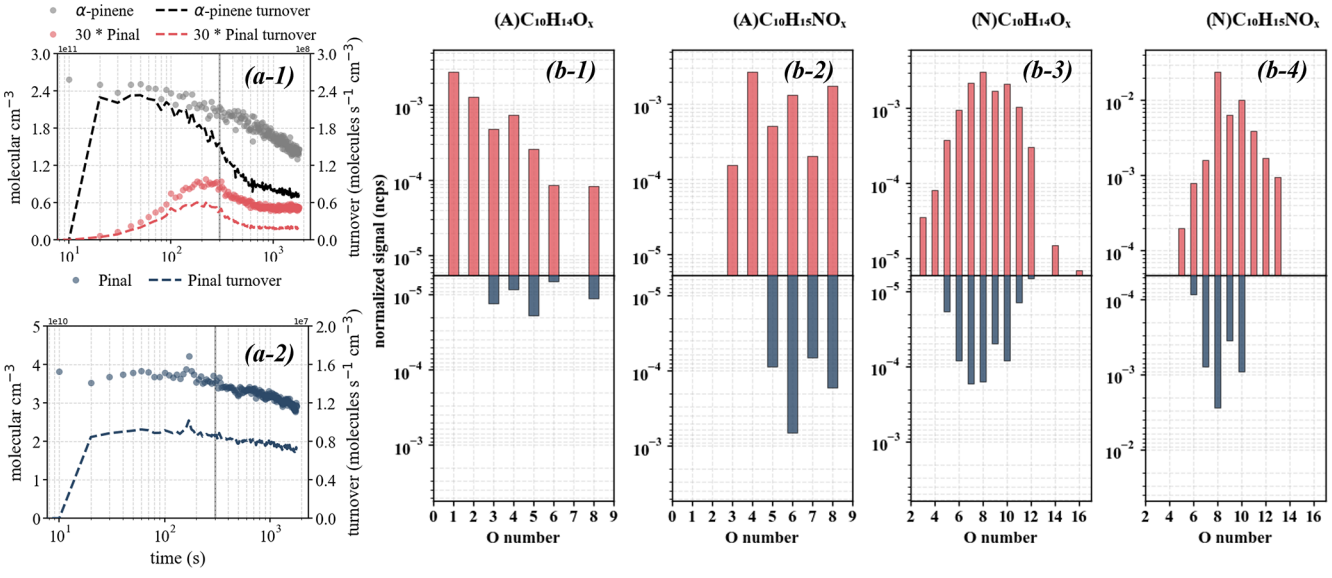

Figure 5. Panel **(a-1)** displays concentrations and turnover of α-pinene and pinonaldehyde (Pinal) during α-pinene photooxidation under high-NO conditions, while panel **(a-2)** represents concentrations and turnover of pinonaldehyde during pinonaldehyde photooxidation under high-NO conditions. Major product distributions are shown in panels **(b-1)** to **(b-4)**. Signals detected in the pinonaldehyde experiment are normalized by the ratio of the pinonaldehyde turnover during the pinonaldehyde experiment to the respective turnover during the α-pinene experiment. The products are separated into four groups: (A)$C_{10}H_{14}O_x$, (A)$C_{10}H_{15}NO_x$, (N)$C_{10}H_{14}O_x$, (N)$C_{10}H_{15}NO_x$, of which (A) and (N) represent signals derived from amine-CIMS and nitrate-CIMS, respectively. Data from α-pinene oxidation and pinonaldehyde oxidation are colored in pink and blue, respectively.

therefore immediately available for reaction with •OH. In contrast, under the α-pinene system, pinonaldehyde had to be formed through α-pinene oxidation before it could undergo further reactions, resulting in a much lower pinonaldehyde turnover during the early stages of the experiment. For $C_{10}H_{15}O_x$•-related HOM detected by nitrate-CIMS the summed signals of the $C_{10}H_{14}O_x$ and $C_{10}H_{15}NO_x$ families under the α-pinene system exceed those of pinonaldehyde system by factors of approximately 20 and 10, respectively. Although pinonaldehyde oxidation contributes to the formation of $C_{10}H_{15}O_x$•-related HOM under high-NO conditions, this contribution is minor and can explain approximately 5 % of the HOM yield observed from α-pinene oxidation. Similarly, for less oxygenated products measured by amine-CIMS, the summed concentrations of the $C_{10}H_{14}O_x$ and $C_{10}H_{15}NO_x$ families were 98 times higher in the α-pinene system, and 6.7 times higher in the pinonaldehyde system.

For highly oxygenated compounds detected by nitrate-CIMS, species containing more than 10 oxygen atoms account for 11 % of the $C_{10}H_{14}O_x$ family and for 13 % of the $C_{10}H_{15}NO_x$ family under α-pinene high-NO condition, whereas their contributions are much lower for pinonaldehyde high-NO conditions (3 % and 5 %, respectively). The initial NO concentrations (Table 1) for two conditions are comparable, and consequently autoxidation rates can be the reason responsible for the differences in HOM distributions. Therefore, for peroxy radicals with more than 9 oxygen atoms the autoxidation chain of $C_{10}H_{15}O_x$• peroxy radicals in pinonaldehyde photooxidation experiments are more easily terminated by NO than for peroxy radicals resulting from α-pinene photooxidation systems. The difference in the product distributions is significant between the two systems. In the pinonaldehyde system, the intensity of the $C_{10}H_{14}O_x$ family is lower than that of the $C_{10}H_{15}NO_x$ family, indicating that the branching towards Reaction (R8) undergoing self-termination is lower than the branching towards Reaction (R6).

For less oxygenated compounds detected by amine-CIMS, the most abundant species in $C_{10}H_{15}NO_x$ family, $C_{10}H_{15}NO_4$,derived from the reaction of $C_{10}H_{15}O_3$• peroxy radicals with NO in the α-pinene system, does not appear in the pinonaldehyde system. Primary peroxy radicals with a formula of $C_{10}H_{15}O_4$• are formed when •OH abstracts a hydrogen atom, mainly from the aldehyde group in pinonaldehyde (Rolletter et al., 2020; Fantechi et al., 2002), as a prerequisite for autoxidation. $C_{10}H_{15}O_3$• form when •OH radicals abstract a hydrogen atom from α-pinene molecules, followed an alkoxy step (Reaction R7), a 6-membered ring opening, and an O_2 molecule addition (Shen et al., 2022). Here, the appearance of $C_{10}H_{15}NO_4$ could be explained by termination reactions between $C_{10}H_{15}O_3$• and NO in the α-pinene system, when the H-abstraction pathway indeed exists. The species detected in amine-CIMS with the formula $C_{10}H_{15}NO_6$ are significantly higher than other compounds in the $C_{10}H_{15}NO_x$ family in the pinonaldehyde system. These species are less important than $C_{10}H_{15}NO_4$ in the α-pinene system. If an alkoxy radical is formed by the reaction of $C_{10}H_{15}O_4$• with NO, followed by H-shift and an O_2 addition, $C_{10}H_{15}O_5$• peroxy radicals will be produced and can be terminated by NO to produce $C_{10}H_{15}NO_6$ species. This is a potential pathway which could be responsible for the significant formation of $C_{10}H_{15}NO_6$ in the pinonaldehyde system.

In summary, clustering analysis shows that $C_{10}H_{15}NO_x$ HOM species exhibit the fastest formation rate among all HOM compounds. They are also faster than first-generation product generation (e.g., pinonaldehyde) in the OH-addition channel under α-pinene high-NO conditions. The intensity of $C_{10}H_{15}O_x$• related HOM ($C_{10}H_{14}O_x$ and $C_{10}H_{15}NO_x$) in the α-pinene photooxidation system is still 11 times higher than those under the pinonaldehyde system although the pinonaldehyde turnover is corrected. In addition, product distributions observed in the α-pinene system differ substantially from those in the pinonaldehyde system, regardless of whether they are detected by nitrate-CIMS or amine-CIMS. Therefore, these findings demonstrate that the H-abstraction pathway, rather than the oxidation of pinonaldehyde, accounts for the formation of $C_{10}H_{15}O_x$• related HOM in the α-pinene system.

4 Conclusions and Atmospheric Implications

In this study a series of photooxidation experiments was conducted under varying NO levels to investigate the effect of NO on the $C_{10}H_{15}O_x$•-related HOM formation in the α-pinene photooxidation system, and to unravel potential formation pathways of these products. The chemical system was brought to a steady state in the dark. Afterwards, reactions were initiated by photolyzing H_2O_2. We focused on early reaction stages (the first hundreds of seconds), during which RO_2• + NO reactions and RO_2• autoxidation reactions dominate the fate of the RO_2•. $C_{10}H_{17}O_x$•-related HOM were dominantly formed via the OH-addition pathway. Product distributions, potential formation pathways, and rates of $C_{10}H_{17}O_x$•-related HOM have been widely and extensively studied (Berndt, 2021; Xu et al., 2019), and our findings on $C_{10}H_{17}O_x$•-related HOM formation are consistent with previous studies. However, potential formation pathways, distributions, and NO dependence of $C_{10}H_{15}O_x$•-related compounds derived from the H-abstraction channel were missing systematic exploration so far.

To constrain the potential contribution of H-abstraction to HOM formation, regimes with and without NO were directly compared, and a separate experiment of pinonaldehyde oxidation under similar conditions was performed. Additionally, measurements by amine-CIMS were used to detect less oxygenated products. Since the photolysis of H_2O_2 was utilized to produce •OH radicals, O_3 did not accumulate during the early reaction stages; therefore, ozonolysis did not

interfere with the •OH pathways. FCM analysis proves that the dominant species in the $C_{10}H_{15}NO_x$ family, $C_{10}H_{15}NO_8$ and $C_7H_9NO_8$, can be distinguished from other species by their fast formation rates in the presence of NO. Pinonaldehyde oxidation can only contribute ∼ 5 % to HOM formation in α-pinene oxidation systems. Therefore, neither ozonolysis nor secondary oxidation can explain the significant formation of $C_{10}H_{15}O_x$•-related HOM, which points to H-abstraction from α-pinene by •OH being the most likely formation pathway.

As illustrated in Figs. S12 and S16, the contribution of the H-abstraction pathway to HOM formation increases with elevated NO levels compared to the OH-addition pathway. The ratios between major $C_{10}H_{15}O_x$•-related HOM and $C_{10}H_{17}Ox$•-related HOM rise with increasing NO concentrations. The ratios of $C_{10}H_{15}O_x$• peroxy radicals to $C_{10}H_{17}O_x$• peroxy radicals are 0.06, 0.83, and 1.42 under NO-free, low-NO, and high-NO conditions, respectively. Similarly, the ratio of $C_{10}H_{15}NO_x$ to $C_{10}H_{17}NO_x$ increases from 0.34 to 0.84 when NO levels increase from low to high. The sum of the major $C_{10}H_{15}O_x$•-related closed-shell HOM ($C_{10}H_{14}O_x$ and $C_{10}H_{15}NO_x$) contributes 24 % and 34 % under low-NO and high-NO conditions, while being negligible under NO-free conditions.

The contribution of H-abstraction related products observed in this study was lower than that reported by Shen and coworkers, who reported a contribution of more than 70 % (Shen et al., 2022). The experiments of the two studies were conducted in different chambers, under different conditions, and with different instrumentations applied. The two chambers could introduce different wall losses of HOM, which can further differ between less oxygenated HOM and highly oxygenated HOM.

In this study the •OH radicals were generated via photolysis of H_2O_2, whereas HONO photolysis was the main source of •OH in Shen et al. (2022). The consecutive reaction between •OH and H_2O_2 in our experiments led to an enhanced production of HO_2• radicals, resulting in an HO_2• concentration of $\sim 4 \times 10^8$ molecule cm^{-3}, which was approximately one order of magnitude higher than that reported by Shen et al. (2022). Also, the NO concentration in Shen et al. was constantly around ∼ 20 ppb, while it was only ∼ 7 ppb before reaction in our study, resulting in a concentration of ∼ 1 ppb during the early-reaction stage. Despite these differences, the contributions of RO_2• + NO reactions were dominant in both studies, accounting for more than 95 % of RO_2• biomolecular losses under high-NO conditions. In addition, we did only consider early reaction stages, during which secondary oxidation was negligible and RO_2• chemistry was dominated by autoxidation and RO_2• + NO reactions. Therefore, the chemical system can be expected to be similar for both studies, at least under high-NO conditions. However, the constantly higher level of NO in the study by Shen et al. (2022) may continuously promote the H-abstraction channel.

The discrepancy may also arise from differences in measurement techniques: Shen et al. (2022) used an Eisele type inlet (Mauldin et al., 1999), while in this study a MION inlet was used (Rissanen et al., 2019). To compare both inlet systems, we conducted an experiment where both types of inlets were simultaneously used to measure the same oxidation systems. The reference system was α-pinene oxidation by •OH, with the addition of NO (Fig. S17). The results indicate that the MION inlets detects a larger fraction of lesser oxygenated HOM (less than eight oxygen atoms) than the Eisele inlet, and that these HOM dominate the $C_{10}H_{17}O_x$•-related HOM family, while the relative contribution of higher oxygenated HOM (more than eight oxygen atoms) was larger in the study by Shen et al. (2022). When only the highly oxygenated HOM compounds are considered, which were analysed by Shen and coworkers, the relative contribution of $C_{10}H_{15}O_x$•-related HOM to the total HOM does increase to 64 %. Therefore, a deeper comparison of the two inlet types may be of interest in the future but is outside the scope of this study.

These findings indicate that the HOM yield attributed to the H-abstraction pathway compared to the OH-addition pathway can be significant and should not be overlooked when assessing the importance of HOM in SOA formation, especially in the presence of NO. Comprehensive product distributions formed through the H-abstraction pathway in α-pinene oxidation are illustrated in this study. HOM species with the formula $C_{10}H_{15}NO_8$, recognized as characteristic indicators of •OH initiated monoterpene oxidation in the presence of NO under daytime atmospheric conditions (Yan et al., 2016; Kulmala et al., 2013), may potentially be attributed to the H-abstraction pathway. However, even the NO concentrations in the low-NO case of this study were higher than those typically observed at Hyytiälä. Therefore, the significance of the H-abstraction pathway under typical low-NO boreal forest conditions remains uncertain and requires further investigation. In contrast, the contribution of the H-abstraction channel to HOM formation is expected to be more pronounced in megacities supposed to be under high NO conditions. The presence of NO not only terminates peroxy radicals and suppresses HOM formation, but also propagates the oxidative radical chain through the formation of alkoxy radicals and their subsequent isomerization, a process that under high NO levels can even compete with autoxidation (Kang et al., 2025). These reactions lead to effective NO-NO_2 conversion and can then become a crucial step to promote O_3 formation. The occurrence of alkoxy steps can also directly be related to O_3 formation in addition to O_3 sensitivity via the ratio of organic nitrate and non-nitrate HOM (Zhang et al., 2024). However, branching ratios towards alkoxy radical formation remain uncertain, when RO_2• reacts with NO. Further investigation is needed to clarify the role of alkoxy processes in both SOA and O_3 formation.

Data availability. The measurement data, the data used for clustering, and the data used as model input in this study are available at: https://doi.org/10.26165/JUELICH-DATA/ZZPLMZ (Wang et al., 2026).

Supplement. The supplement related to this article is available online at https://doi.org/10.5194/acp-26-11153-2026-supplement.

Author contributions. HW and HS prepared the manuscript with contributions by SK, TFM, DRW, DZ, and SRZ. HW, AZ, MB, YB, RW, SK, QH, TH, and SRZ conducted the experiments and performed the measurements. HW, HS, and SK analyzed the data. HW performed the model calculations. The compiled data set was interpreted by HW, HS, DZ, and SRZ. All co-authors discussed the results and commented on the manuscript.

Competing interests. At least one of the (co-)authors is a member of the editorial board of *Atmospheric Chemistry and Physics*. The peer-review process was guided by an independent editor, and the authors also have no other competing interests to declare.

Disclaimer. Publisher's note: Copernicus Publications remains neutral with regard to jurisdictional claims made in the text, published maps, institutional affiliations, or any other geographical representation in this paper. The authors bear the ultimate responsibility for providing appropriate place names. Views expressed in the text are those of the authors and do not necessarily reflect the views of the publisher.

Acknowledgements. The authors would like to thank the editor, the two anonymous reviewers, and Shunyu Yao for their constructive comments that helped to improve the manuscript.

Financial support. This research was supported by the Federal Ministry of Education and Research (BMBF, Germany) under the FONA strategy "Research for Sustainability" through the ACTRIS-D project (funding code: 01LK200010). Hongru Shen and Defeng Zhao would like to thank for funding support from the Shanghai Pilot Program for Basic Research-Fudan University 21TQ1400100 (22TQ010).

The article processing charges for this open-access publication were covered by the Forschungszentrum Jülich.

Review statement. This paper was edited by Jason Surratt and reviewed by two anonymous referees.

References

Albrecht, S. R., Novelli, A., Hofzumahaus, A., Kang, S., Baker, Y., Mentel, T., Wahner, A., and Fuchs, H.: Measurements of hydroperoxy radicals (HO2) at atmospheric concentrations using bromide chemical ionisation mass spectrometry, Atmos. Meas. Tech., 12, 891–902, https://doi.org/10.5194/amt-12-891-2019, 2019.

Atkinson, R. and Arey, J.: Atmospheric Degradation of Volatile Organic Compounds, Chem. Rev., 103, 4605–4638, https://doi.org/10.1021/cr0206420, 2003.

Baker, Y., Kang, S., Wang, H., Wu, R., Xu, J., Zanders, A., He, Q., Hohaus, T., Ziehm, T., Geretti, V., Bannan, T. J., O'Meara, S. P., Voliotis, A., Hallquist, M., McFiggans, G., Zorn, S. R., Wahner, A., and Mentel, T. F.: Impact of HO_2/RO_2 ratio on highly oxygenated α-pinene photooxidation products and secondary organic aerosol formation potential, Atmos. Chem. Phys., 24, 4789–4807, https://doi.org/10.5194/acp-24-4789-2024, 2024.

Berndt, T.: Peroxy Radical Processes and Product Formation in the OH Radical-Initiated Oxidation of alpha-Pinene for Near-Atmospheric Conditions, J. Phys. Chem. A, 125, 9151–9160, https://doi.org/10.1021/acs.jpca.1c05576, 2021.

Berndt, T.: Peroxy Radical and Product Formation in the Gas-Phase Ozonolysis of alpha-Pinene under Near-Atmospheric Conditions: Occurrence of an Additional Series of Peroxy Radicals O,O-C(10)H(15)O(O(2))(y)O(2) with y = 1-3, J. Phys. Chem. A, 126, 6526–6537, https://doi.org/10.1021/acs.jpca.2c05094, 2022.

Berndt, T., Richters, S., Jokinen, T., Hyttinen, N., Kurten, T., Otkjaer, R. V., Kjaergaard, H. G., Stratmann, F., Herrmann, H., Sipila, M., Kulmala, M., and Ehn, M.: Hydroxyl radical-induced formation of highly oxidized organic compounds, Nat. Commun., 7, https://doi.org/10.1038/ncomms13677, 2016.

Berndt, T., Mentler, B., Scholz, W., Fischer, L., Herrmann, H., Kulmala, M., and Hansel, A.: Accretion Product Formation from Ozonolysis and OH Radical Reaction of alpha-Pinene: Mechanistic Insight and the Influence of Isoprene and Ethylene, Environ. Sci. Technol., 52, 11069–11077, https://doi.org/10.1021/acs.est.8b02210, 2018.

Bianchi, F., Kurten, T., Riva, M., Mohr, C., Rissanen, M. P., Roldin, P., Berndt, T., Crounse, J. D., Wennberg, P. O., Mentel, T. F., Wildt, J., Junninen, H., Jokinen, T., Kulmala, M., Worsnop, D. R., Thornton, J. A., Donahue, N., Kjaergaard, H. G., and Ehn, M.: Highly Oxygenated Organic Molecules (HOM) from Gas-Phase Autoxidation Involving Peroxy Radicals: A Key Contributor to Atmospheric Aerosol, Chem. Rev., 119, 3472–3509, https://doi.org/10.1021/acs.chemrev.8b00395, 2019.

Campello, R. J. G. B. and Hruschka, E. R.: A fuzzy extension of the silhouette width criterion for cluster analysis, Fuzzy Set. Syst., 157, 2858–2875, https://doi.org/10.1016/j.fss.2006.07.006, 2006.

Ehn, M., Thornton, J. A., Kleist, E., Sipila, M., Junninen, H., Pullinen, I., Springer, M., Rubach, F., Tillmann, R., Lee, B., Lopez-Hilfiker, F., Andres, S., Acir, I. H., Rissanen, M., Jokinen, T., Schobesberger, S., Kangasluoma, J., Kontkanen, J., Nieminen, T., Kurten, T., Nielsen, L. B., Jorgensen, S., Kjaergaard, H. G., Canagaratna, M., Maso, M. D., Berndt, T., Petaja, T., Wahner, A., Kerminen, V. M., Kulmala, M., Worsnop, D. R., Wildt, J., and Mentel, T. F.: A large source of low-

volatility secondary organic aerosol, Nature, 506, 476–479, https://doi.org/10.1038/nature13032, 2014.

Eisele, F. L. and Tanner, D. J.: Measurement of the gas phase concentration of H_2SO_4 and methane sulfonic acid and estimates of H_2SO_4 production and loss in the atmosphere, J. Geophys. Res.-Atmos., 98, 9001–9010, https://doi.org/10.1029/93JD00031, 1993.

Fantechi, G., Vereecken, L., and Peeters, J.: The OH-initiated atmospheric oxidation of pinonaldehyde: Detailed theoretical study and mechanism construction, Phys. Chem. Chem. Phys., 4, 5795–5805, https://doi.org/10.1039/b205901k, 2002.

Iyer, S., Reiman, H., Moller, K. H., Rissanen, M. P., Kjaergaard, H. G., and Kurten, T.: Computational Investigation of RO(2) + HO(2) and RO(2) + RO(2) Reactions of Monoterpene Derived First-Generation Peroxy Radicals Leading to Radical Recycling, J. Phys. Chem. A, 122, 9542–9552, https://doi.org/10.1021/acs.jpca.8b09241, 2018.

Jenkin, M. E., Saunders, S. M., and Pilling, M. J.: The tropospheric degradation of volatile organic compounds: a protocol for mechanism development, Atmos. Environ., 31, 81–104, https://doi.org/10.1016/S1352-2310(96)00105-7, 1997.

Jenkin, M. E., Valorso, R., Aumont, B., and Rickard, A. R.: Estimation of rate coefficients and branching ratios for reactions of organic peroxy radicals for use in automated mechanism construction, Atmos. Chem. Phys., 19, 7691–7717, https://doi.org/10.5194/acp-19-7691-2019, 2019.

Jimenez, J. L., Canagaratna, M. R., Donahue, N. M., Prevot, A. S. H., Zhang, Q., Kroll, J. H., DeCarlo, P. F., Allan, J. D., Coe, H., Ng, N. L., Aiken, A. C., Docherty, K. S., Ulbrich, I. M., Grieshop, A. P., Robinson, A. L., Duplissy, J., Smith, J. D., Wilson, K. R., Lanz, V. A., Hueglin, C., Sun, Y. L., Tian, J., Laaksonen, A., Raatikainen, T., Rautiainen, J., Vaattovaara, P., Ehn, M., Kulmala, M., Tomlinson, J. M., Collins, D. R., Cubison, M. J., Dunlea, E. J., Huffman, J. A., Onasch, T. B., Alfarra, M. R., Williams, P. I., Bower, K., Kondo, Y., Schneider, J., Drewnick, F., Borrmann, S., Weimer, S., Demerjian, K., Salcedo, D., Cottrell, L., Griffin, R., Takami, A., Miyoshi, T., Hatakeyama, S., Shimono, A., Sun, J. Y., Zhang, Y. M., Dzepina, K., Kimmel, J. R., Sueper, D., Jayne, J. T., Herndon, S. C., Trimborn, A. M., Williams, L. R., Wood, E. C., Middlebrook, A. M., Kolb, C. E., Baltensperger, U., and Worsnop, D. R.: Evolution of Organic Aerosols in the Atmosphere, Science, 326, 1525–1529, https://doi.org/10.1126/science.1180353, 2009.

Kang, S., Wildt, J., Pullinen, I., Vereecken, L., Wu, C., Wahner, A., Zorn, S. R., and Mentel, T. F.: Formation of highly oxygenated organic molecules from α-pinene photooxidation: evidence for the importance of highly oxygenated alkoxy radicals, Atmos. Chem. Phys., 25, 15715–15740, https://doi.org/10.5194/acp-25-15715-2025, 2025.

Kiendler-Scharr, A., Wildt, J., Dal Maso, M., Hohaus, T., Kleist, E., Mentel, T. F., Tillmann, R., Uerlings, R., Schurr, U., and Wahner, A.: New particle formation in forests inhibited by isoprene emissions, Nature, 461, 381–384, https://doi.org/10.1038/nature08292, 2009.

Koss, A. R., Canagaratna, M. R., Zaytsev, A., Krechmer, J. E., Breitenlechner, M., Nihill, K. J., Lim, C. Y., Rowe, J. C., Roscioli, J. R., Keutsch, F. N., and Kroll, J. H.: Dimensionality-reduction techniques for complex mass spectrometric datasets: application to laboratory atmospheric organic oxidation experiments, Atmos. Chem. Phys., 20, 1021–1041, https://doi.org/10.5194/acp-20-1021-2020, 2020.

Kroll, J. H., Donahue, N. M., Jimenez, J. L., Kessler, S. H., Canagaratna, M. R., Wilson, K. R., Altieri, K. E., Mazzoleni, L. R., Wozniak, A. S., Bluhm, H., Mysak, E. R., Smith, J. D., Kolb, C. E., and Worsnop, D. R.: Carbon oxidation state as a metric for describing the chemistry of atmospheric organic aerosol, Nat. Chem., 3, 133–139, https://doi.org/10.1038/NCHEM.948, 2011.

Kulmala, M., Kontkanen, J., Junninen, H., Lehtipalo, K., Manninen, H. E., Nieminen, T., Petäjä, T., Sipilä, M., Schobesberger, S., Rantala, P., Franchin, A., Jokinen, T., Järvinen, E., Äijälä, M., Kangasluoma, J., Hakala, J., Aalto, P. P., Paasonen, P., Mikkilä, J., Vanhanen, J., Aalto, J., Hakola, H., Makkonen, U., Ruuskanen, T., Mauldin, R. L., Duplissy, J., Vehkamäki, H., Bäck, J., Kortelainen, A., Riipinen, I., Kurtén, T., Johnston, M. V., Smith, J. N., Ehn, M., Mentel, T. F., Lehtinen, K. E. J., Laaksonen, A., Kerminen, V.-M., and Worsnop, D. R.: Direct Observations of Atmospheric Aerosol Nucleation, Science, 339, 943–946, https://doi.org/10.1126/science.1227385, 2013.

Lee, B. H., Iyer, S., Kurtén, T., Varelas, J. G., Luo, J., Thomson, R. J., and Thornton, J. A.: Ring-opening yields and auto-oxidation rates of the resulting peroxy radicals from OH-oxidation of α-pinene and β-pinene, Environ. Sci. Atmos., 3, 399–407, https://doi.org/10.1039/d2ea00133k, 2023.

Luo, H., Vereecken, L., Shen, H., Kang, S., Pullinen, I., Hallquist, M., Fuchs, H., Wahner, A., Kiendler-Scharr, A., Mentel, T. F., and Zhao, D.: Formation of highly oxygenated organic molecules from the oxidation of limonene by OH radical: significant contribution of H-abstraction pathway, Atmos. Chem. Phys., 23, 7297–7319, https://doi.org/10.5194/acp-23-7297-2023, 2023.

Mauldin, R. L., Tanner, D. J., Heath, J. A., Huebert, B. J., and Eisele, F. L.: Observations of H2SO4 and MSA during PEM-Tropics-A, J. Geophys. Res.-Atmos., 104, 5801–5816, https://doi.org/10.1029/98jd02612, 1999.

Mentel, Th. F., Wildt, J., Kiendler-Scharr, A., Kleist, E., Tillmann, R., Dal Maso, M., Fisseha, R., Hohaus, Th., Spahn, H., Uerlings, R., Wegener, R., Griffiths, P. T., Dinar, E., Rudich, Y., and Wahner, A.: Photochemical production of aerosols from real plant emissions, Atmos. Chem. Phys., 9, 4387–4406, https://doi.org/10.5194/acp-9-4387-2009, 2009.

Mentel, T. F., Springer, M., Ehn, M., Kleist, E., Pullinen, I., Kurtén, T., Rissanen, M., Wahner, A., and Wildt, J.: Formation of highly oxidized multifunctional compounds: autoxidation of peroxy radicals formed in the ozonolysis of alkenes – deduced from structure–product relationships, Atmos. Chem. Phys., 15, 6745–6765, https://doi.org/10.5194/acp-15-6745-2015, 2015.

Peng, J., Hu, M., Guo, S., Du, Z., Zheng, J., Shang, D., Levy Zamora, M., Zeng, L., Shao, M., Wu, Y.-S., Zheng, J., Wang, Y., Glen, C. R., Collins, D. R., Molina, M. J., and Zhang, R.: Markedly enhanced absorption and direct radiative forcing of black carbon under polluted urban environments, P. Natl. Acad. Sci. USA, 113, 4266–4271, https://doi.org/10.1073/pnas.1602310113, 2016.

Piletic, I. R. and Kleindienst, T. E.: Rates and Yields of Unimolecular Reactions Producing Highly Oxidized Peroxy Radicals in the OH-Induced Autoxidation of alpha-Pinene, beta-Pinene, and Limonene, J. Phys. Chem. A, 126, 88–100, https://doi.org/10.1021/acs.jpca.1c07961, 2022.

Rissanen, M. P., Kurten, T., Sipila, M., Thornton, J. A., Kangasluoma, J., Sarnela, N., Junninen, H., Jorgensen, S., Schallhart, S., Kajos, M. K., Taipale, R., Springer, M., Mentel, T. F., Ruuskanen, T., Petaja, T., Worsnop, D. R., Kjaergaard, H. G., and Ehn, M.: The formation of highly oxidized multifunctional products in the ozonolysis of cyclohexene, J. Am. Chem. Soc., 136, 15596–15606, https://doi.org/10.1021/ja507146s, 2014.

Rissanen, M. P., Mikkilä, J., Iyer, S., and Hakala, J.: Multi-scheme chemical ionization inlet (MION) for fast switching of reagent ion chemistry in atmospheric pressure chemical ionization mass spectrometry (CIMS) applications, Atmos. Meas. Tech., 12, 6635–6646, https://doi.org/10.5194/amt-12-6635-2019, 2019.

Rolletter, M., Kaminski, M., Acir, I.-H., Bohn, B., Dorn, H.-P., Li, X., Lutz, A., Nehr, S., Rohrer, F., Tillmann, R., Wegener, R., Hofzumahaus, A., Kiendler-Scharr, A., Wahner, A., and Fuchs, H.: Investigation of the α-pinene photooxidation by OH in the atmospheric simulation chamber SAPHIR, Atmos. Chem. Phys., 19, 11635–11649, https://doi.org/10.5194/acp-19-11635-2019, 2019.

Rolletter, M., Blocquet, M., Kaminski, M., Bohn, B., Dorn, H.-P., Hofzumahaus, A., Holland, F., Li, X., Rohrer, F., Tillmann, R., Wegener, R., Kiendler-Scharr, A., Wahner, A., and Fuchs, H.: Photooxidation of pinonaldehyde at ambient conditions investigated in the atmospheric simulation chamber SAPHIR, Atmos. Chem. Phys., 20, 13701–13719, https://doi.org/10.5194/acp-20-13701-2020, 2020.

Shen, H., Vereecken, L., Kang, S., Pullinen, I., Fuchs, H., Zhao, D., and Mentel, T. F.: Unexpected significance of a minor reaction pathway in daytime formation of biogenic highly oxygenated organic compounds, Sci. Adv., 8, eabp8702, https://doi.org/10.1126/sciadv.abp8702, 2022.

Vereecken, L. and Peeters, J.: Theoretical Study of the Formation of Acetone in the OH-Initiated Atmospheric Oxidation of α-Pinene, J. Phys. Chem. A, 104, 11140–11146, https://doi.org/10.1021/jp0025173, 2000.

Vereecken, L. and Peeters, J.: Decomposition of substituted alkoxy radicals–part I: a generalized structure-activity relationship for reaction barrier heights, Phys. Chem. Chem. Phys., 11, 9062–9074, https://doi.org/10.1039/b909712k, 2009.

Vereecken, L. and Peeters, J.: A structure-activity relationship for the rate coefficient of H-migration in substituted alkoxy radicals, Phys. Chem. Chem. Phys., 12, 12608–12620, https://doi.org/10.1039/c0cp00387e, 2010.

Vereecken, L., Muller, J. F., and Peeters, J.: Low-volatility poly-oxygenates in the OH-initiated atmospheric oxidation of alpha-pinene: impact of non-traditional peroxyl radical chemistry, Phys. Chem. Chem. Phys., 9, 5241–5248, https://doi.org/10.1039/b708023a, 2007.

Wang, H., Baker, Y., Shen, H. R., Wu, R. R., Kang, S. A., Zhao, D. F., Wahner, A., Zorn, S. R., and Mentel, T. F.: Decomposition of Clusters of Oxygenated Compounds with NO by Applying Voltage Scanning to Chemical Ionization Mass Spectrometry in Steady-State Experiments, Environ. Sci. Tech. Lett., https://doi.org/10.1021/acs.estlett.4c00276, 2024.

Wang, H., Shen, H., Zhao, D., Kang, S., Wu, R., Baker, Y., He, Q., Zanders, A., Bachner, M., Worsnop, D. R., Hohaus, T., Mentel, T. F., and Zorn, S. R.: Supplementary data for "Exploring the Hydrogen Abstraction Pathway in HOM Formation from α-pinene Photooxidation Systems under Varying NO Conditions" (V1), Jülich DATA [data set], https://doi.org/10.26165/JUELICH-DATA/ZZPLMZ, 2026.

Wu, R., Vereecken, L., Tsiligiannis, E., Kang, S., Albrecht, S. R., Hantschke, L., Zhao, D., Novelli, A., Fuchs, H., Tillmann, R., Hohaus, T., Carlsson, P. T. M., Shenolikar, J., Bernard, F., Crowley, J. N., Fry, J. L., Brownwood, B., Thornton, J. A., Brown, S. S., Kiendler-Scharr, A., Wahner, A., Hallquist, M., and Mentel, T. F.: Molecular composition and volatility of multi-generation products formed from isoprene oxidation by nitrate radical, Atmos. Chem. Phys., 21, 10799–10824, https://doi.org/10.5194/acp-21-10799-2021, 2021.

Wu, R., Zorn, S. R., Kang, S., Kiendler-Scharr, A., Wahner, A., and Mentel, T. F.: Application of fuzzy c-means clustering for analysis of chemical ionization mass spectra: insights into the gas phase chemistry of NO_3-initiated oxidation of isoprene, Atmos. Meas. Tech., 17, 1811–1835, https://doi.org/10.5194/amt-17-1811-2024, 2024.

Xu, L., Moller, K. H., Crounse, J. D., Otkjaer, R. V., Kjaergaard, H. G., and Wennberg, P. O.: Unimolecular Reactions of Peroxy Radicals Formed in the Oxidation of alpha-Pinene and beta-Pinene by Hydroxyl Radicals, J. Phys. Chem. A, 123, 1661–1674, https://doi.org/10.1021/acs.jpca.8b11726, 2019.

Yan, C., Nie, W., Äijälä, M., Rissanen, M. P., Canagaratna, M. R., Massoli, P., Junninen, H., Jokinen, T., Sarnela, N., Häme, S. A. K., Schobesberger, S., Canonaco, F., Yao, L., Prévôt, A. S. H., Petäjä, T., Kulmala, M., Sipilä, M., Worsnop, D. R., and Ehn, M.: Source characterization of highly oxidized multifunctional compounds in a boreal forest environment using positive matrix factorization, Atmos. Chem. Phys., 16, 12715–12731, https://doi.org/10.5194/acp-16-12715-2016, 2016.

Zhang, J., Zhao, J., Luo, Y., Mickwitz, V., Worsnop, D., and Ehn, M.: On the potential use of highly oxygenated organic molecules (HOMs) as indicators for ozone formation sensitivity, Atmos. Chem. Phys., 24, 2885–2911, https://doi.org/10.5194/acp-24-2885-2024, 2024.